Sedimentology (2018) doi: 10.1111/sed.12528

Grain-size variability within a mega-scale point-bar system, False River, Louisiana

PETER D. CLIFT*†, ELIZABETH D. OLSON*, ALEXANDRA LECHNOWSKYJ*, MARY GRACE MORAN*, ALLISON BARBATO* and JUAN M. LORENZO*
**Department of Geology and Geophysics, Louisiana State University, Baton Rouge, LA 70803, USA (E-mail: pclift@lsu.edu)*
†Coastal Studies Institute, Louisiana State University, Baton Rouge, LA 70803, USA

ABSTRACT

Point bars formed by meandering river systems are an important class of sedimentary deposit and are of significant economic interest as hydrocarbon reservoirs. Standard point-bar models of how the internal sedimentology varies are based on the structure of small-scale systems with little information about the largest complexes and how these might differ. Here a very large point bar (>25·0 m thick and 7·5 × 13·0 km across) on the Mississippi River (USA) was examined. The lithology and grain-size characteristics at different parts of the point bar were determined by using a combination of coring and electrical conductivity logging. The data confirm that there is a general fining up-section along most parts of the point bar, with a well-defined transition from massive medium-grained sands below about 9 to 11 m depth up into interbedded silts and fine–medium sand sediment (inclined heterolithic strata). There is also a poorly defined increase in sorting quality at the transition level. Massive medium sands are especially common in the region of the channel bend apex and regions upstream of that point. Downstream of the meander apex, there is much less evidence for fining up-section. Finer sediment accumulated more readily after the establishment of a compound bar in the later stages of construction, at the terminal apex and in the bar tail. This work implies that the best reservoir sands are likely to be located in the centre of the point bar, deposited in a simple bar system. Reservoir quality decreases towards the bar edge. The early-stage channel plug is largely composed of coarsening-upward cycles of silt to clay and is dominated by clay and clayey silt material with poor reservoir characteristics.

Keywords Electrical conductivity, grain size, meander, Mississippi, point bar.

INTRODUCTION

Mega-point bars

Alluvial floodplains are a major class of continental sedimentary depositional setting (Miall, 2006). Sediments preserved in such locations can form thick successions in the geological record where subsidence allows their long-term preservation [for example, the Old Red Sandstone of the British Isles (Marriott & Wright, 1993); the Beaufort Formation of the Karroo Basin (Smith, 1990); the Indo-Gangetic Plain (Gibling *et al.*, 2005); and the Rocky Mountain foreland basin (McCarthy *et al.*, 1997)]. Meandering rivers form a significant sub-category of all such deposits, although their preservation potential may be less than braided rivers that have been argued to dominate the geological record (Gibling, 2006). Whether this is actually correct or not has recently been called into question (Hartley *et al.*, 2015). Although the basic

processes that operate during meander loop migration and the formation of point-bar systems have been established for some time (Daniel, 1971; Brice, 1974; Jackson, 1976; Miall, 1985), it is unclear whether the largest examples (>20 m thick) are simply enlarged versions of the better-studied medium-scale and small-scale systems. In particular, existing models make predictions about grain-size variability both laterally and vertically in a meandering river system (Jackson, 1976; Smith, 1987; Yan *et al.*, 2017), based on grain size being linked to flow velocity, which is generally higher in the thalweg and on the outer cut bank and slower on the inner bank especially downstream of the apex (Leopold *et al.*, 1964; Allen, 1965) (Fig. 1). In addition, flow velocity and grain size are expected to change during meander cut-off as flow is diverted into a new channel (Zinger *et al.*, 2011) or during times of point-bar reorientation, when the direction of apex migration changes (rotation), affecting downstream current patterns. A number of factors may influence the internal structure and grain size of point-bar complexes. Hampson *et al.* (2012) have argued that the lithofacies within a point bar reflect the interplay of allogenic and autogenic processes, including climate change, tectonics and eustasy. In particular, grain size and sedimentary facies are intimately linked with discharge, channel dimensions, sinuosity and flow velocities which, in turn, are related to sediment supply, changes in base level and regional topographic gradient (Schumm, 1993; Bogaart & Van Balen, 2000; Knighton, 2014).

The largest point bars are formed in the lower reaches of major continental-scale rivers where the floodplains are wide and there are few obstacles to meander bend migration (Gibling, 2006; Miall, 2006). However, their preservation potential is limited where subsidence is slow. Simple upscaling of existing models may not be appropriate when predicting grain size in the largest point bars because a number of controls, including sea level, climate, basin subsidence and tectonics may affect the larger, longer-lived point bars, but such processes are typically not significant for smaller examples (Tornqvist, 1993; Blum & Törnqvist, 2000; Hooke, 2008; Frascati & Lanzoni, 2009). The largest point bars are modelled to form over periods of 900 to 1500 years (Schwenk *et al.*, 2015), while recent observations of the middle reaches of the Mississippi record bend apex migration rates of 0·3 to 6·0 m year^{-1} on point bars that are typically 500 to 1500 m across and up to 2 km long (Robinson, 2013). A large point bar (>10 km measured in a downdip direction from the bend apex to the cut-off point) would thus be expected to be constructed over at least 1600 years when migration rates were 6·0 m year^{-1} or less. This means that in order to understand the life cycle of an entire point bar it is necessary to core and image the interior to determine how the river flow evolution has affected sediment type and grain-size characteristics. This is typically hard to do because few ancient examples provide exposure in depth and planform and those that do are mostly much smaller scale systems, for example, the Scalby Formation in the UK (Ghinassi & Ielpi, 2015), the Ferron Sandstone of Utah (Wang & Bhattacharya, 2017), the Caspe Formation of the Ebro Basin, Spain (Cuevas Martinez *et al.*, 2010) and the Cerro Bacino Formation of the Canadon Asfalto

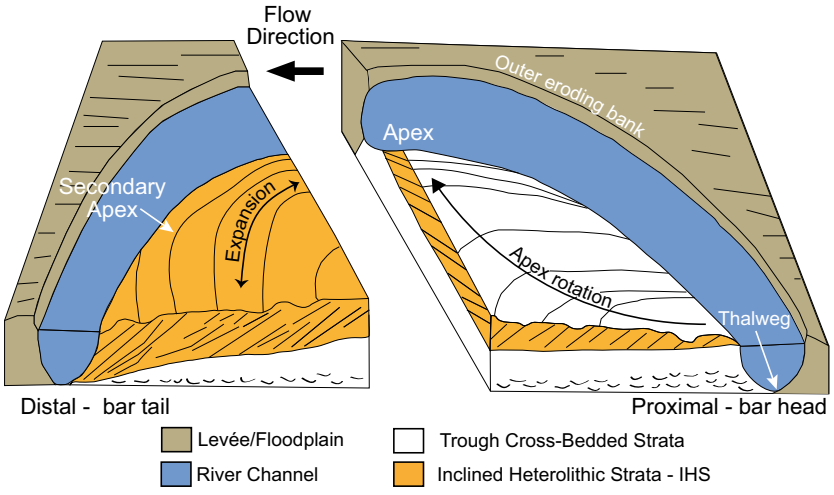

Fig. 1. Schematic illustration of a point-bar complex showing the major architectural elements discussed in this study, modified after the Fustic *et al.* (2012) model for the McMurray Formation. This model is based from concepts originally published by Smith (1985), Wood (1989) and Wightman & Pemberton (1997). Note the rotation of apex trajectory with time and formation of multiple apices late in the point-bar accretion.

Basin, Argentina (Foix *et al.*, 2012). As a result, determining the internal structure of point bars has been attempted on modern systems where imaging can be attempted using seismic or ground penetrating radar (Bridge *et al.*, 1995) but this, in turn, is typically constrained to thinner point bars that can be imaged in their entirety. In any case coring is required to confirm lithologies and to acquire detailed grain-size information because there is significant variability in the lithofacies within a point bar so that no single facies model can account for the range of stratigraphic complexity in fluvial point-bar deposits (Gibling, 2006; Ghinassi & Ielpi, 2015; Ghinassi *et al.*, 2016).

This study combines grain-size analysis of cored sediment with electrical conductivity data to constrain variability within a Holocene Mississippi River mega-point bar. For the purpose of this study this is defined to mean one >20 m thick. Such an example of a modern analogue can provide the channel geometries, flow rates and environmental conditions that are generally unavailable from outcrop studies. The specific objectives of this study were: (i) to determine if the point bar shows fining upward sequences in upstream and downstream parts of the point bar; (ii) to test whether grain size fines downstream around the meander; (iii) to constrain the grain size response to changes in meander development, especially reorientation events; and (iv) to assess the response of the point bar to meander cut-off.

Significance

Point-bar deposits can be of significant economic, as well as scientific interest. In particular, fluvial sediments can form effective hydrocarbon reservoirs if the porosity and permeability allow the ready flow of fluids (Fielding & Crane, 1987; Dreyer *et al.*, 1992; Miall, 2006). For example, meandering river sediments form the reservoir of huge bitumen accumulations of Alberta, Canada, where the Cretaceous Fort McMurray Formation is the host rock (Wightman & Pemberton, 1997). Other productive meandering river petroleum reservoirs include those in the Widuri field in the Java Sea (Carter, 2003), in the Little Creek field of Mississippi (Werren *et al.*, 1990) and in the Jonah Gas field of Wyoming (Shanley, 2004). Detailed understanding of the porosity and permeability characteristics of such units is critical to their efficient production and is largely a function of the grain-size variability (Ajdukiewicz & Lander, 2010). Key questions include whether porous and permeable sand-rich reservoir units are interconnected within a point bar or if they are separated by muddy impermeable layers that would interfere with the ability to produce hydrocarbons from a wide area of the formation. Such issues are also important to the extraction of water from aquifers and to predict the possible spread of contaminants through an aquifer. Although numerical models have been developed that can help predict such characteristics based on the geometries observed in three-dimensional seismic surveys (Yan *et al.*, 2017; Colombera *et al.*, 2018), such models are best used when the lateral extent of facies and grain-size variability is well-constrained. Seismic methods can provide the geometry of the meander externally and sometimes internally (Hubbard *et al.*, 2011; Alqahtani *et al.*, 2015) but are weak at constraining lithology.

Existing point-bar models

Within a meander belt, many primary and secondary depositional environments exist, reflecting shifts in the river over time. Whether accumulation or erosion takes place is a function of the relative position of the thalweg, the point of highest velocity in river flow (Fig. 1) (Fisk, 1947; Gouw, 2007). The geometry of a meandering river channel means that the thalweg is closer to the outer bend of the meander, the cut bank, than the inner bend. This is especially true near the apex of a meander bend, while the channel is more symmetrical around the inflection (Julien & Wargadalam, 1995). In plan view, the cut bank is concave and is the area with the greatest amount of erosion which is achieved through bank caving, and collapse of material into the channel (Allen, 1965; Collinson, 1986). Alternatively, the inner, convex bank, may be viewed as the location of active accumulation. Point bars are often considered to follow a general model of formation, in which sediment eroded from the cut bank (outer curve of the channel) is then deposited on the opposite leeward side of the channel. Sediment accumulating on this convex bank ultimately builds a depositional feature called a point bar as the channel migrates across the floodplain (Fisk, 1947; Allen, 1965). This process, along with shifting of the position of the thalweg and river channel, is a mechanism by which a meandering

river strives to reach a steady state. This process continues until the river achieves a cut-off, which results in the largest heterogeneity in the resultant deposits when cut-off is achieved through a neck cut-off, i.e. when the main stream connects across the point bar at the closest point between bends, resulting in meander loop abandonment. Alternatively, cut-off may be achieved during floods as a result of chute cut-off when a more direct route can be established around a point bar that would incise across the existing deposits (Constantine *et al.*, 2010). In this most traditional form of model meander migration is mostly viewed as occurring perpendicular to river flow but this neglects the tendency of meanders to migrate downstream, especially as their amplitude increases (Parker *et al.*, 1982). Furthermore, heterogeneities in the floodplain, most notably clay-rich channel fills, can impede migration or stabilize this in a particular direction (Parker & Andrews, 1986; Hudson & Kesel, 2000). Modelling indicates that meander loop migration represents a balance between deposition and stabilization of the inner bank and erosion of the outer bank through a cyclic process of undercutting of more erodible sand-rich sediment and episodic collapse of an overlying more coherent vegetated clay-rich top layer (Parker *et al.*, 2010).

The direction of meander migration is also important in controlling lithology within the point bar, i.e. whether the meander expands mostly laterally, perpendicular to the flow direction or with the direction of flow if lateral migration is confined either by a valley wall or by strong, cohesive sediments (Smith *et al.*, 2009, 2011). Expansion of the meander is the process by which the curvature and distance around the meander increases as migration proceeds. Meanders can migrate either through lateral migration perpendicular to the regional river flow direction and/or downstream in the direction of flow. If the direction of propagation of the bend apex changes during migration then this process is called rotation (Brice, 1974; Ghinassi & Ielpi, 2015; Yan *et al.*, 2017). A recent synthesis suggests that both downstream migrating point bars and laterally expanding point bars (where the radius of meander increases as the meander migrates) share several characteristics but that bar-tail deposits differ in downstream migrating point bars (Ghinassi *et al.*, 2016). In these locations fine-grained counter-point bars or coarse-grained eddy-accretion deposits may be found.

Many meander bends and their point bars comprise a relatively simple loop in the channel but the situation can be more complex. A point bar is said to be 'composite' when it is formed by a set of conformable lateral accretion units, which in plan-view corresponds to a group of parallel scroll bars or ridges and swales (Diaz-Molina, 1993). A compound point bar is one that comprises a number of smaller meanders within a larger bend and where meanders may be cut-off by chutes during high water stages (Miall, 1985). This study treats the overall False River point bar, located in south Louisiana in the Mississippi River lower reaches as a single complex, including both simple and compound phases of development. The study also considers individual subunits that can be separated using the re-orientation surfaces seen in the scroll bar topography (Fig. 2). When assessing up-section or downstream variability this study attempts to compare data within a single accretionary unit, or at least with reference to the apex at the time of sedimentation rather than location within the overall complex.

Point-bar deposits generally fine upward because of the gradient in current strength in the channel, although this is not always the case. Fining-upward sequences are only poorly developed or absent in the coarser-grained upstream parts of bars in the Scalby Formation (Ielpi & Ghinassi, 2014), in the Wabash River of Illinois (Jackson, 1976) and in the Scottish River Endrick (Bluck, 1971). Counter point-bar deposits that form downstream of the bar apex in the modern Peace River of Alberta, Canada (*ca* 12 m thick) show a thickening of the silt-dominated upper bar (Smith *et al.*, 2009). Despite this there is no clear fining-upward trend in the Peace River bars, a characteristic they also share with counter point bars in the McMurray Formation (20 to 45 m thick channels) (Smith *et al.*, 2009). The upper part of the bar stratigraphy is often composed of interbedded sands, silts and clays. These sediments are then recognized as the laterally accreting units in which the original accretionary angle is preserved (Thomas *et al.*, 1987). This angle represents the dip of the front of the bar and is a measure of the inclination of the inner bank of the river channel bend. This interbedded zone is sometimes referred to as the Inclined Heterolithic Strata (IHS). Variations in the IHS correspond to the scroll bar topography (Fig. 2) (Gibling & Rust, 1993). In contrast, the lower portion of the point bar is characterized by trough cross-bedded sandy strata (Allen,

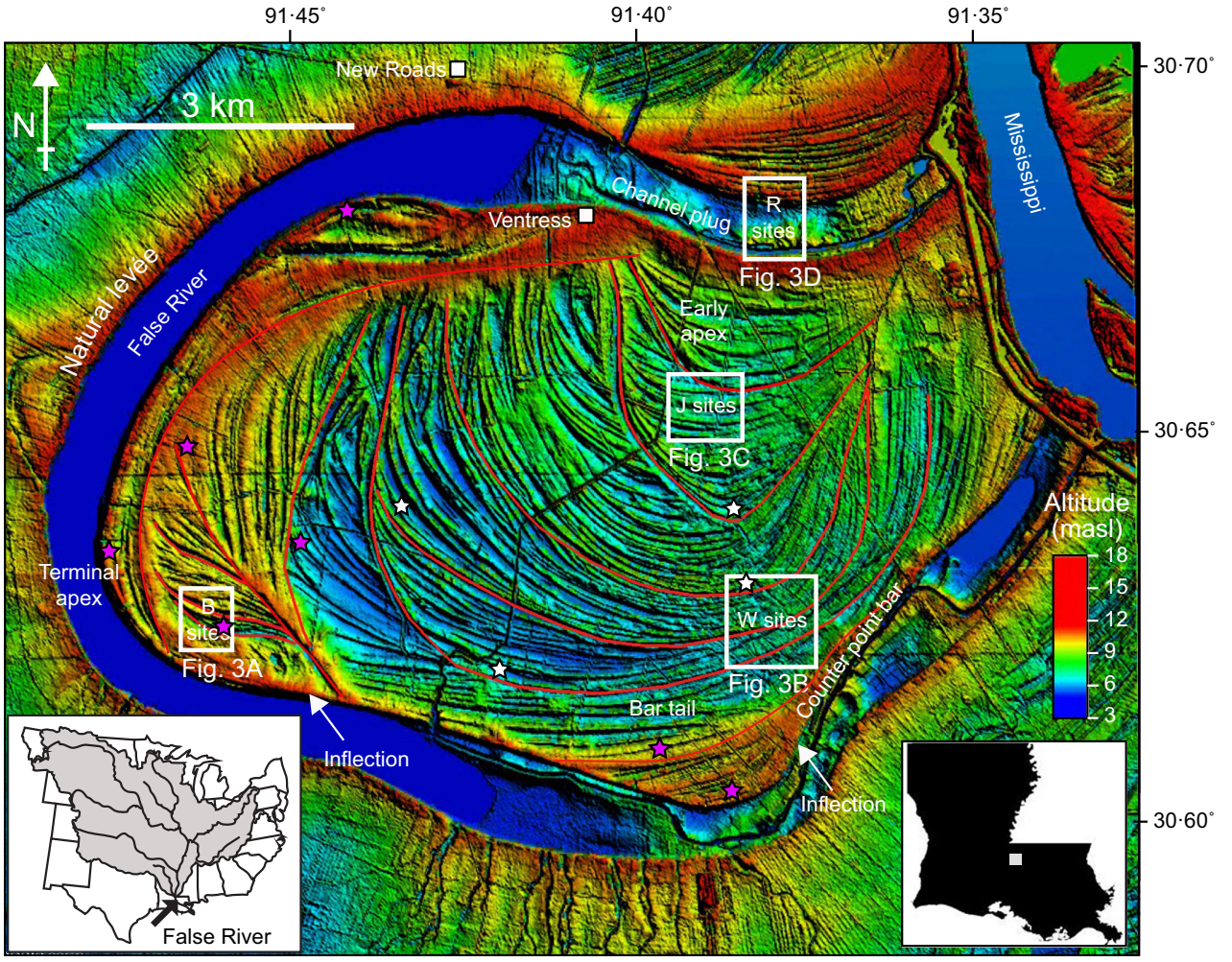

Fig. 2. Colour-shaded topographic map of the False River point-bar system next to the Mississippi River in south Louisiana. Right inset map shows outline of Louisiana with grey box showing the location of False River. Left inset map shows the Mississippi catchment with the major tributaries together with the outlines of the US states. Black arrow shows the location of False River. Colour scale depicts altitude above sea level. Red solid lines indicate major re-orientation surfaces within the point bar defined on the basis of the light detection and ranging (LIDAR) topography allowing the construction of the point bar to be broken up into a series of discrete stages. White stars show the apex of the point bar for different stages of the bar construction. Pink stars show the apices of the point bar when it is in a compound phase of construction. Resolution of the False River digital elevation model (DEM) image is 1/9 arc-second (3 m cell size) (Gesch *et al.*, 2002).

1963) that are generally more homogenous in lithology (McGowen & Garner, 1970). This part of the bar is composed dominantly of sand with no marked bounding surfaces that are delineated by mud drapes, as would be typical of IHS. As well as fining upward, simple point-bar models predict a downstream fining in grain size, resulting in a downstream increase in the thickness of the IHS. The IHS development has been linked to tidal activity in several locations because tides provide some of the current strength variation required to deposit the finer grained units (Choi, 2011; Johnson & Dashtgard, 2014; Shiers *et al.*, 2014). However, there are many examples where IHS form in purely fluvial settings under the influence of secondary or counter currents, especially linked to the development of counter point bars (Smith *et al.*, 2009).

Point bars are expected to be coarsest upstream of the bar apex, where the fastest current runs close to the accreting bank of the point bar, and finest downstream of that point in the bar tail (Fig. 1), as the maximum current erodes the outer banks. Within this general trend there

is the potential for sharp changes in grain size across reorientation surfaces (Nanson, 1980; Smith, 1987), especially if the bar apex moves a significant distance between sub-units. Significant grain-size changes are also predicted during the meander cut-off process. This is important not only for predicting quality in point-bar hydrocarbon reservoirs, but also for being able to recognize where in such a point-bar complex a given fluvial sequence might be located in the case where there is incomplete outcrop or seismic information.

Heterogeneities are formed in a point bar when continuous sedimentation is interrupted, such as between formation of accretionary units. Breaks in periods of semi-continuous sedimentation might follow flooding events causing rotation or erosion via chute channels. At the highest level either neck or chute cut-off events are the largest possible such breaks and occur when the stream is effectively isolated from the point bar, allowing the meandering channel loop to be preserved as an oxbow lake (Fisk, 1947; Saucier, 1969; Toonen *et al.*, 2012). Point bars are then separated from one another by the abandoned channels filled by a combination of coarse sand to silt grade fluvial sediments and finer grained, silt–clay-rich material deposited in the oxbow lake.

Abandonment occurs as the result of the river constantly striving to shorten its course, which in turn is influenced by the type of sediment in the point bar (Zinger *et al.*, 2011). There are two types of meander cut-off event: neck cut-off and chute cut-off. Neck cut-off tends to occur more quickly, even during the time of one flood event, when the concave banks of adjacent meanders erode towards one another and the narrow neck of the point bar is breached (Willis & Tang, 2010). Chute cut-off, on the other hand, can be a significantly slower process that may take tens of years to finish (Saucier, 1974). During a major flood event, flow has the opportunity to cut across a point bar through a swale and thus scour a major channel leading to abandonment of the pre-existing channel. On the Mississippi River, Saucier (1974) estimated that neck cut-offs outnumber chute cut-offs by at least 20:1.

Prior to final cut-off other events may affect the internal sedimentology of a point bar and result in large-scale divisions. Simple models involving cut-bank erosion and sedimentation on the opposite side assume a constant river sediment load and relatively uniform construction (Allen, 1965; Hickin, 1974; Miall, 1985). Such models lack the fine scale heterogeneity seen in more advanced models (Smith, 1985; Wightman & Pemberton, 1997; Willis & Tang, 2010; Labrecque *et al.*, 2011; Fustic *et al.*, 2012). In later models of larger scale systems, the assumption of a uniform sediment load is replaced by seasonal or longer-term discharge variability (Fustic *et al.*, 2012). This could include pulses related to spring snow melting, monsoonal summer rains, or longer-term changes linked to climatic phenomena such as El Niño. Tidal influence too can be important and has been invoked in the formation of finer grained layers in the IHS (Hubbard *et al.*, 2011; Díez-Canseco *et al.*, 2014), although the location of False River close to the top of the Mississippi tidal backwater makes this process unlikely to be important in this case. Flooding events are crucial in forming discontinuities in a point bar (Fisk, 1947; Fustic, 2007; Fustic *et al.*, 2012). The largest scale discontinuities imply a reorientation and break in the migration direction of the point bar following some event that caused partial erosion of the earlier point bar (Musial *et al.*, 2012). Such a break provides the opportunity for a significant change in the sediment type being deposited at any given part of the point bar.

FALSE RIVER CASE STUDY

This study addresses the False River point bar that lies between the 'False River' oxbow lake and the modern Mississippi in southern Louisiana (Fig. 2). Although False River lies within the tidal backwater zone of the Mississippi it is only 82 km from the top of this zone that extends 490 km from the river mouth (Chatanantavet *et al.*, 2012), so that tidal effects are considered to be minimal (Lamb *et al.*, 2012). This meander experienced cut-off in 1722 (Sternberg, 1956). The point bar directly overlies coarse sand and gravels deposited during the Last Glacial Maximum (LGM) when sea level was lower and the Mississippi was entrenched as a braided river system in a broad cut valley that has been progressively filled as sea level rose until *ca* 6 ka (Blum & Roberts, 2012). Aggradation is dated to have begun in the southern area of the Mississippi valley about 8 ka (Gouw & Autin, 2008).

Neck cut-off was determined as the means of abandonment by Fisk (1947), based on aerial photographs of the river in 1947 – these images show that the oxbow lake is bounded on one side by an accretionary point bar, and on the

other by a natural levée (Fig. 2). Levée deposits overlie inclined point-bar sediments that sit on top of what Saucier (1969) considers undifferentiated meander belt deposits and substratum deposits, with sharp boundaries between these sediments and the abandoned channel fill on either side. However, this early interpretation shows a division between the inclined upper bar and lower 'undifferentiated' deposits. Saucier (1969) does not fully recognize the stratigraphic complications between the upper and lower bar, as that study incorrectly grouped the lower bar sand package as part of the LGM substratum deposits. There are sharp boundaries between the channel belt sands and floodplain clay-rich sediments (Fisk, 1947), as well as a well-developed crevasse splay developed on the southern side of the meander loop (Farrell, 1987). Migration of the False River point bar towards the south-west after a rotation from a more north to south trajectory resulted in a coarsening upward sequence within the overbank deposits and the development of surficial splay deposits.

The large-scale architecture of the point bar is evident in the high resolution light detection and ranging (LIDAR) digital elevation model (DEM) imagery (Fig. 2) and is used to distinguish the erosional and depositional features on the surface of the alluvial plain. The high resolution of the DEM image (1/9 arc-second; 3 m cell size) reveals fine-scale surface topography (including reorientation surfaces, ridges and swales), the abandoned channel ties, oxbow lake and natural levées.

METHODS

This study is based on three primary data sets: DEM image analysis, grain-size analysis of cored sediment samples and *in situ* electrical conductivity logs. All eleven cores and the ten geophysical logs considered in this study were collected using a Geoprobe® 6610DT mobile rig. Sediment coring recovered 146 m in three areas (Figs 2 and 3); in the north in a location close to the bar apex during the early part of point-bar accretion (J sites), close to the apex at the time of cut-off (B sites) and a transect of sites that lie in the bar tail during the latter phases of accretion (W sites) (Fig. 2). In addition, three cores were drilled across the northern channel plug (R sites) (Fig. 3; Table 1). Three more cores were collected at the terminal apex B sites and another three on the bar tail W sites because these were anticipated to have more lithological heterogeneity compared to the early bar apex J sites. Coring was biased towards the top of each section (ranging from 11·0 m at Site B1 to 25·7 m at Site R3) because recovery is efficient at those depths and because the working models discussed above predict that this is where the bulk of the lithological heterogeneity would lie.

Electrical conductivity

Sediment electrical conductivity is a measurement of the ability of the grains (and pore fluid) to carry an electrical current. Because ions conduct electrical current more efficiently, sediments, such as clays, that have a high ion content will have a higher conductivity value (Revil & Glover, 1998). In contrast, coarse-grained sediments such as sand, will have a lower value. Because of this, sediment electrical conductivity is a useful tool for detecting lithology and potentially allows for horizontal correlation in areas where multiple sites can be measured (McCall, 1996). The electrical conductivity equipment consists of a probe connected through a series of rods to a real-time display, with the probe being forced into the sediment by a hydraulic percussion hammering method. Ten electrical conductivity logs were collected during this work.

Grain-size analysis

In this study, 462 samples were collected throughout the False River system with 107 grain-size samples collected from the B sites, 64 samples from the J sites, 141 samples from the W sites and 150 samples from the R sites: 1 cm^3 grain-size samples were collected *ca* every 30 cm, and were then sieved in an 850 μm sieve with 5·75 ml of $NaPO_3$. Samples were then centrifuged at 35 rpm for 30 min to remove the supernatant. A solution was created by adding 2 ml of $NaPO_3$ and 5 ml of H_2O_2, placed in the vortex and then left to sit for 30 min, followed by *ca* 10 h in a hot bath. This preparation method was modified from that of Hülse & Bentley (2012). Samples were then analyzed by a Beckman-Coulter LS 1320W Laser Diffraction Particle Size Analyzer (Beckman Coulter Inc., Brae, CA, USA) at Louisiana State University. Data is provided ranging from 0·37 to 1821 μm. To ensure that equal amounts of each sample were analyzed, the standard operating procedure for the samples here was with an obscuration in the target range of *ca* 8 to 11%, with minimal use of auto-dilution techniques.

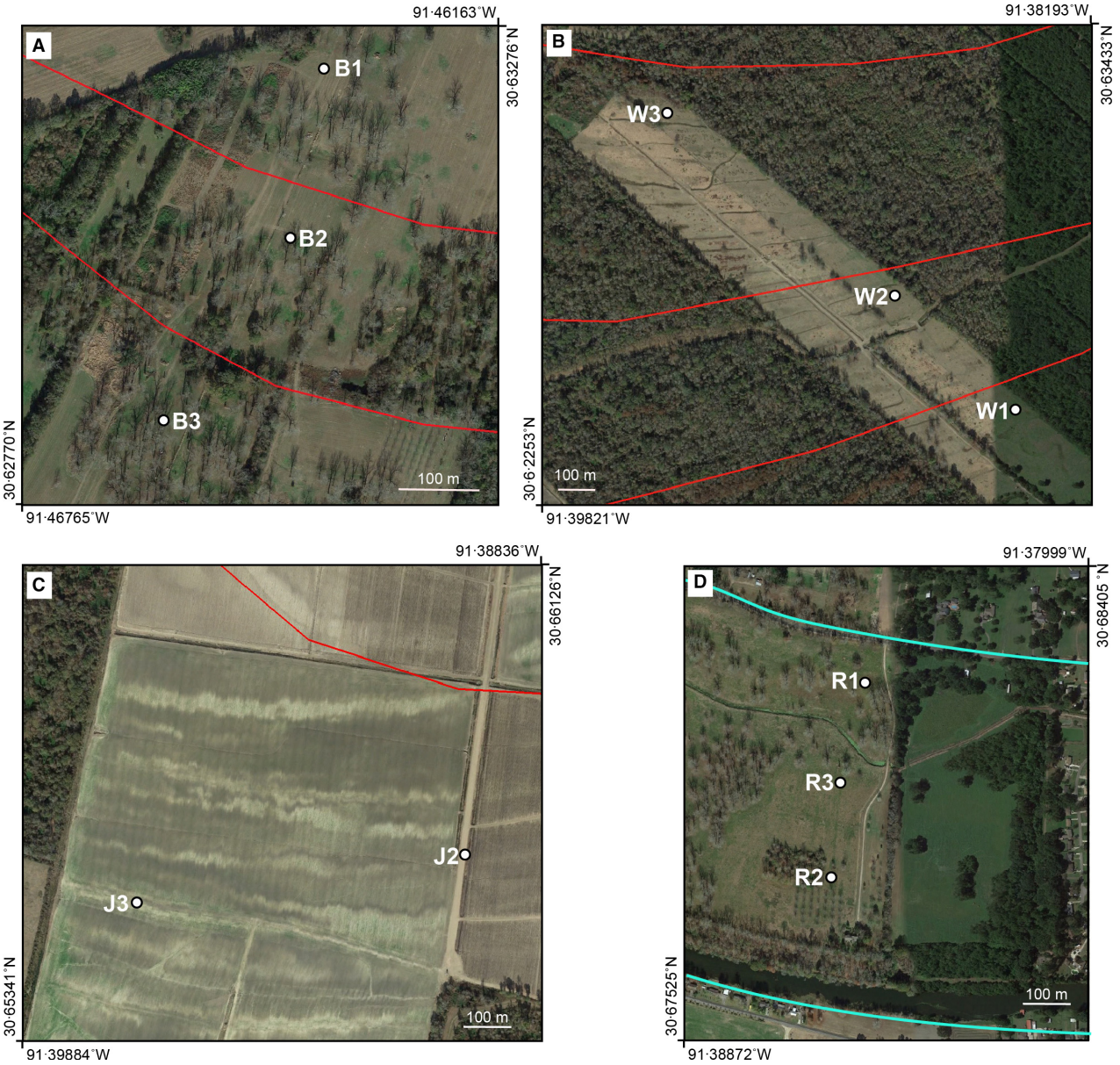

Fig. 3. Aerial photographs of the four areas cored and logged as part of this study. Locations of the core sites are shown relative to the main reactivation surfaces shown as red lines. Locations of individual areas within the point bar are shown in Fig. 2. Precise GPS coordinates of the sites are provided in Table 1. (A) B area sites located in the terminal bar apex, (B) W area sites located in the bar tail, and (C) J area sites located in the early apex. The channel plug area (D) shows the edge of the former channel as solid blue lines.

Preliminary analysis was concerned with univariate grain-size parameters and the associated moment statistics. Kurtosis and skewness, or the asymmetry of distribution, refers to moment parameters (Tanner, 1991). Positive skewness is defined by Folk & Ward (1974) and Blatt *et al.* (1980) to describe samples with a significant fine tail. For further analysis, end-member modelling was conducted using *AnalySize*, a MATLAB© based software for grain-size unmixing developed by Paterson & Heslop (2015). End member analysis of sediment grain-size has previously proven effective in isolating provenance of different populations, as well as resolving different depositional mechanisms (Weltje & Prins, 2003, 2007). The minimum number of coefficients of determination (r^2) was calculated for scenarios with the number of end members varying between 2 and 10. In this process, r^2 was taken for every grain-size specimen ($n = 459$). After, the mean and

Table 1. Global positioning system (GPS) coordinates and depths of cored intervals at the sites considered in this study.

Site	North (°)	West (°)	Cored intervals (m)
W1	30·69750	91·39172	0 to 21·94
W2	30·72569	91·42664	0 to 13·41
W3	30·77081	91·49200	0 to 21·94
B1	30·77317	91·58883	0 to 13·41 and 19·51 to 21·94
B2	30·75500	91·59317	0 to 9·75 and 13·41 to 19·51
B3	30·73531	91·60900	0 to 12·19
J2	30·71072	91·44936	0 to 13·41
J3	30·70336	91·51675	0 to 13·41
R1	30·68194	91·38486	0 to 12·19
R2	30·67831	91·38561	0 to 13·72
R3	30·68008	91·38539	0 to 24·38

median of all combined values of r^2 were taken and a mean/median r^2 was created. The graph of the number of end-members (q) versus mean/median r^2 was the primary tool for determining the minimum number of end members, as experiments with synthetic mixtures have shown that the true number of end members (q) corresponds to the value of q at the point of inflection on the (q–$r^2_{\mathrm{me\ (di)\ an}}$) curve (Prins & Weltje, 1999). Using these r^2 statistics, the False River dataset is sufficiently described as mixtures of four end-members (EM1 to EM4) (Fig. 4E and F). Type EM1 is a poorly sorted muddy-fine silt sediment and EM2 is a well-sorted silt. Types EM3 and EM4 are dominated, respectively, by well-sorted fine and medium sands. The preferred end members in this study are common to all samples and allow differences between sites and depths to be compared.

RESULTS

Light detection and ranging topography

Analysis of the DEM image allows the coarse scale construction history of the point bar to be determined and the evolving location of the bar apex to be defined between reorientation surfaces (Fig. 2). These reorientation surfaces represent times when the direction of apex migration sharply changed (rotation), probably following erosion during a flood event. The meander loop expanded substantially from its earliest state to a broad loop by midway through its construction. The LIDAR image shows that there is a change from a simple uni-apex geometry to a multi-apex compound geometry in the latter stages of bar accretion (Fig. 2). The B sites and W1 are located within this compound part of the complex, while the other sites precede this transition.

Grain-size analysis

Sediments from all sites show a range of grain sizes that are commonly seen to show a strong fine-grained component, coupled with a complex coarser component that can be broken down into sub-peaks (Fig. 4A to D). The general character of the sediment types can be assessed using the classification scheme of Folk (1954) (Fig. 5). Although there is a wide spread in sediment type there is strong clustering towards silt and sandy silt, with rather fewer sand-rich sediments and a uniform lack of clay-dominated material. This plot does not directly show any preference in grain size between the sites and so each core site is examined in detail to identify more subtle trends within and across the point bar (Figs 6 to 9).

Lithology in the early apex region

Coring was limited to the top half of the point bar at Sites J2 and J3 in the early bar apex (Fig. 6). The electrical conductivity logging is supportive of the concept that below the depth of coring, sediments are mostly homogenous and sandy, as shown by low, uniform conductivity values that contrast with the more variable character of the electrical conductivity log above *ca* 15 m depth (Fig. 6). Simple correlation between grain-size data and electrical conductivity values is hard to establish. Although there are sections where grain size is coarse and electrical conductivity is low, as predicted (for example, >10·5 m at Site J2; Fig. 6), Site J3 shows low electrical conductivity values but relatively fine mean grain size below 9 m. The grain-size data indicate that the muddier top is thicker at J3 (*ca* 13 m) compared to *ca* 10·5 m at J2, although this is at odds with the electrical conductivity data (Fig. 6). The very finest material that is defined as the bar top comprises the top 3 m in each case, with the underlying interbedded clays, silts and sands being defined as the IHS. The division between these two units is drawn on the basis of the grain-size analyses coupled with the visual core descriptions. Because the grain-size analyses are only every 30 cm, precedence is given to the visual

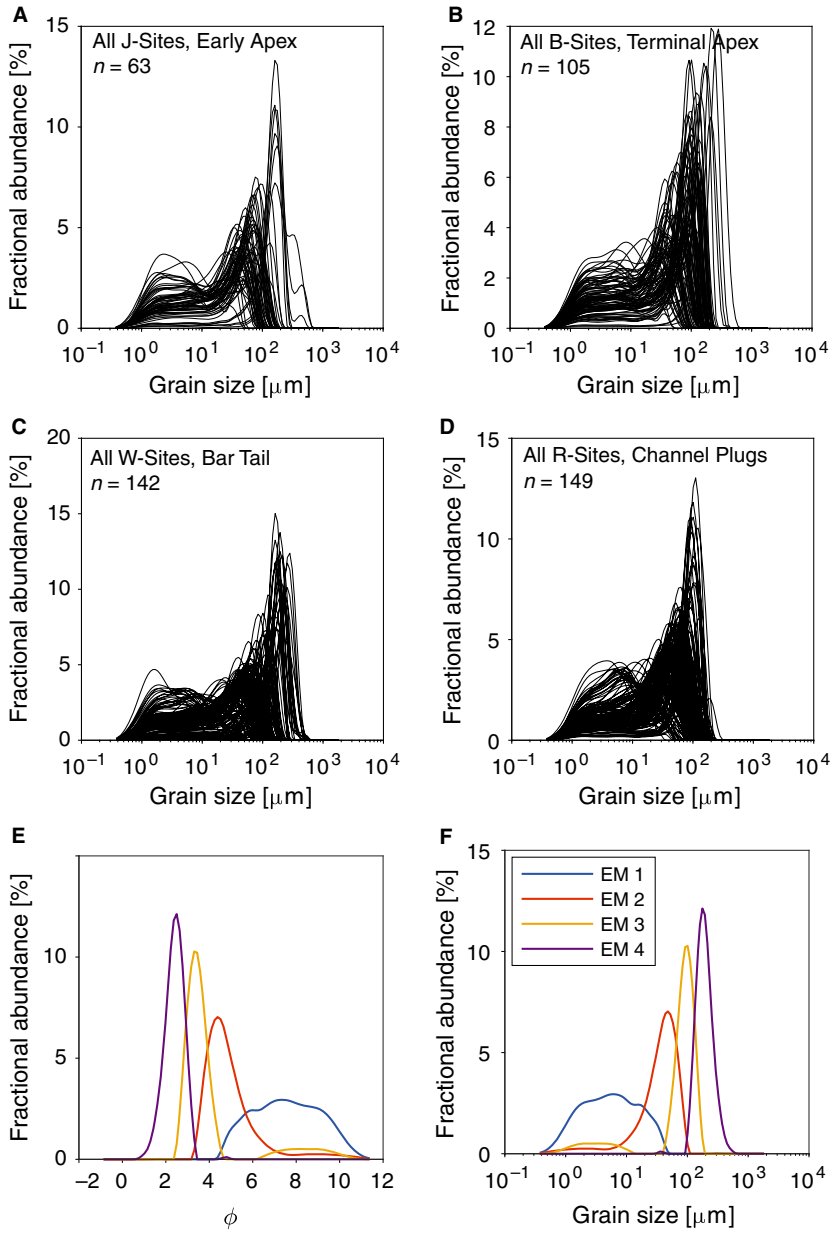

Fig. 4. Grain-size measurements from the four study areas showing all sediments from each on a logarithmic micron scale: (A) J-sites, early apex; (B) B-sites, terminal apex; (C) W-sites, bar tail; and (D) R-sites, channel plugs. (E) and (F) End member (EM) grain-size populations derived from *AnalySize* and which account for >95% of the variability measured in samples from all cored sediments. End members are shown with grain size expressed as width in (E) ϕ units and (F) microns.

descriptions where the two are not in perfect accord. Site J2 shows the clearest trend to fining upward, which is rapid below 10·5 m (Fig. 6), as shown in the mean and mode grain size, as well as the appearance of EM4 in significant volumes. Sorting also improves below this level. In contrast, although the sediment at Site J3 has a similar IHS unit, bottoming at 9 m depth, it does not show a clear vertical trend in grain size based on the particle size analysis (Fig. 6). The visual description and the electrical conductivity log suggest that there is more sand down-section than might be implied from the grain-size analysis alone.

Lithology in the final apex region

Sites B1 and B3 located at the terminal apex are clearly more fine-grained than the sediments seen at J2 and J3 (Figs 6 and 7). Site B2 is more massive and sand-rich based on the visual description and electrical conductivity logs, at least below 4 m depth, although the grain-size analysis points to the sand being consistently finer than that seen in the lower parts of Site J2. Correlation of electrical conductivity data and grain-size measurements is hard to establish because electrical conductivity values are *ca* 20 millisiemens m^{-1} through

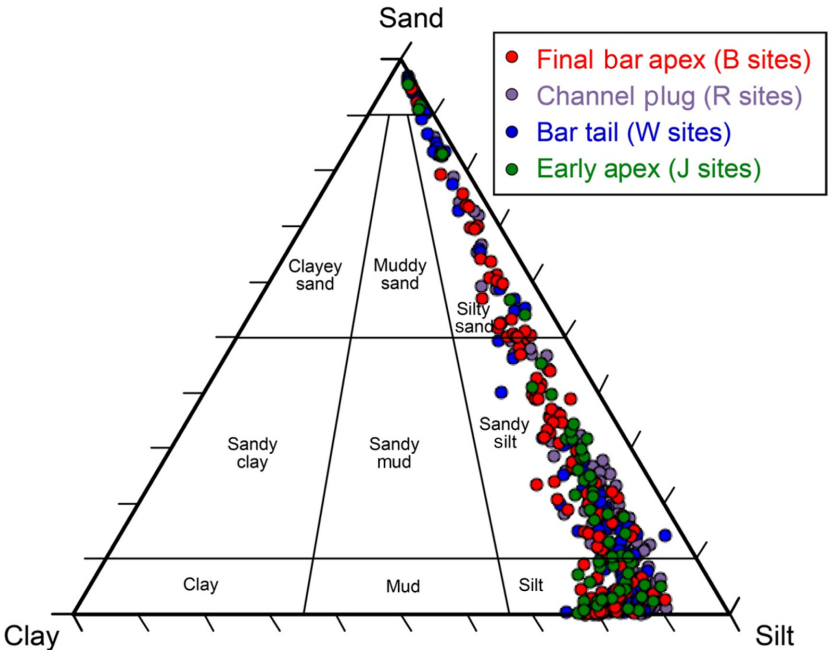

Fig. 5. Grain-size range of all sediment samples from the False River point bar and associated channel plugs shown on the scheme of Folk (1954).

much of the silt-dominated sections at Sites B1 and B2 (Fig. 7). The coarser grained interbeds at 9 to 13 m depth at Site B1 are associated with only slightly lower electrical conductivity values. However, at Site B3 the scattered mean and mode grain sizes correlate with a highly variable electrical conductivity record: EM3 dominates the lower part of the cored section at Site B2, rather than EM4, as seen at Site J2 (Figs 6 and 7). The electrical conductivity logs are also indicative of a mostly sandy section below the bar top at Site B2, with only moderate amounts of muddy interbedding within the IHS. In contrast, both core and electrical conductivity data show muddy interbeds in the otherwise sandy section below *ca* 5 m depth at Site B1 (Fig. 7). Grain-size analysis does not show a clear trend of fining-up or decreased sorting below the bar top at Site B1. Therefore, it is unclear if there is any meaningful transition from IHS into a more massive base. The absence of a clear grain-size trend is even more pronounced at Site B3 (Fig. 7). Coring confirms that silty and muddy sediments dominate the upper 11 m at Site B3 and although there is more sand below 7 m it is still interbedded with poorly sorted muds. The electrical conductivity log indicates that the entire section down to 28 m depth may comprise sediment of this character. Although sand beds are seen throughout they are interlayered with frequent muddy intervals.

Lithology in the bar tail region

Sites in the bar tail (W1, W2 and W3) show the greatest degrees of variability within a limited area (Fig. 8). The oldest site, W3, has some similarity to Site J2 (Figs 6 and 8). The bar top is *ca* 2 m thick, with the base of the IHS at 11 m. Below that depth the core is sand-dominated, with large proportions of EM4 and a mode frequently of medium sand. This coarser section is associated with lower electrical conductivity values as might be anticipated. There is a clear fining upward within the IHS (Fig 8). Sorting is variable but with higher kurtosis common below 7 m at Site W3. There are indications of sparse interbeds of finer grained material below the IHS, but the section is essentially sand-dominated. Moving towards the south-west and the exterior of the point bar there is limited evidence at Site W2 because electrical conductivity logging and coring only penetrated to 13 m depth (Fig. 8). However, within that range grain size remains very fine. The first sandy interval is seen below 4 m depth, although even below that level EM1 and EM2 still dominate. Silty sediment represents the vast majority of measured grain-size means and modes and there is no trend to up-section fining at Site W2 (Fig. 8). The youngest site in this transect (W1) shows one of the finest grained sections from the whole study. There are intermittent sand beds, but these are sparse and heavily interbedded with

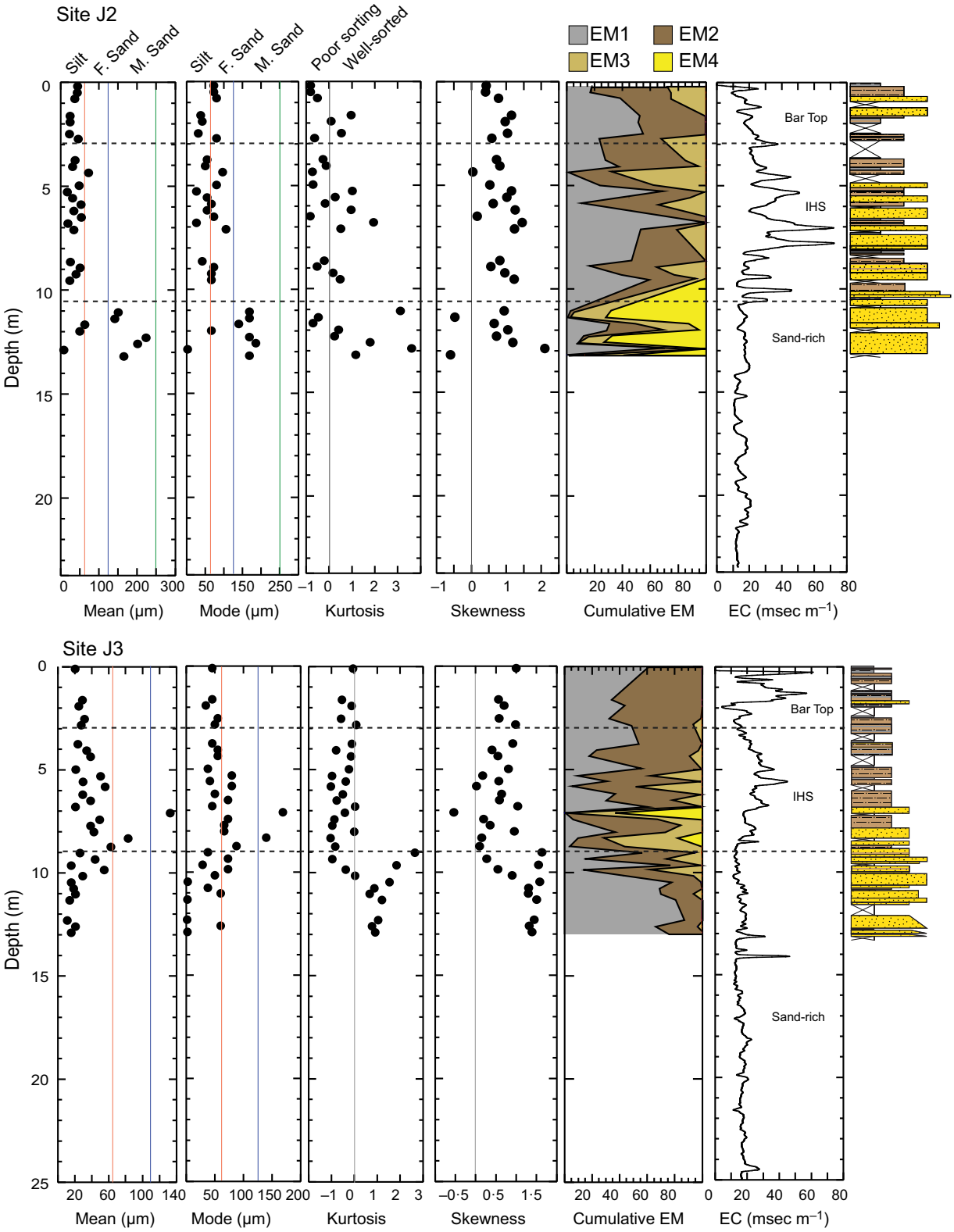

Fig. 6. Downhole plots of grain-size variability at the early apex sites J2 and J3. See Figs 1 and 7 for location. The mean, mode, kurtosis and skewness of the sediments from each site for which grain-size characteristics were measured are displayed. A further column shows the breakdown of end members derived by processing through *AnalySize* software, as well as the electrical conductivity downhole log (electrical conductivity). All of these parameters are compared with the visual core description shown on the right-hand side of each figure.

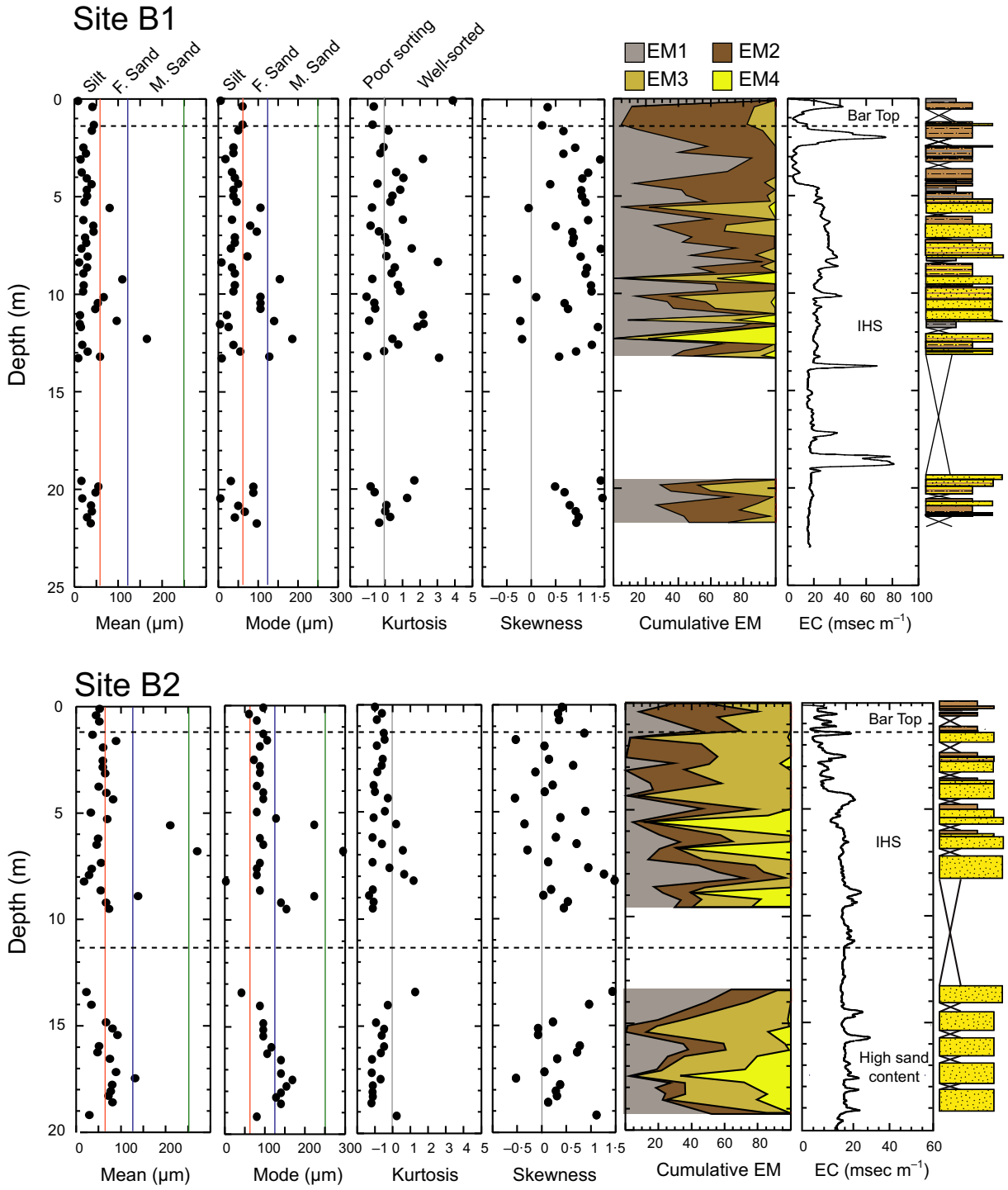

Fig. 7. Downhole plots of grain-size variability at the terminal apex sites B1, B2 and B3. See Figs 1 and 7 for location. The mean, mode, kurtosis and skewness of the sediments from each site for which grain-size characteristics were measured are displayed. A further column shows the breakdown of end members derived by processing through *AnalySize* software, as well as the electrical conductivity downhole log (electrical conductivity). All of these parameters are compared with the visual core description shown on the right-hand side of each figure.

silty and clay-rich layers down to 19 m where the base of the IHS was inferred, the thickest of all recorded in this work (Fig. 8). The interbedded fine and coarse-grained sediments below 8 m depth correlate with an especially variable electrical conductivity record, with

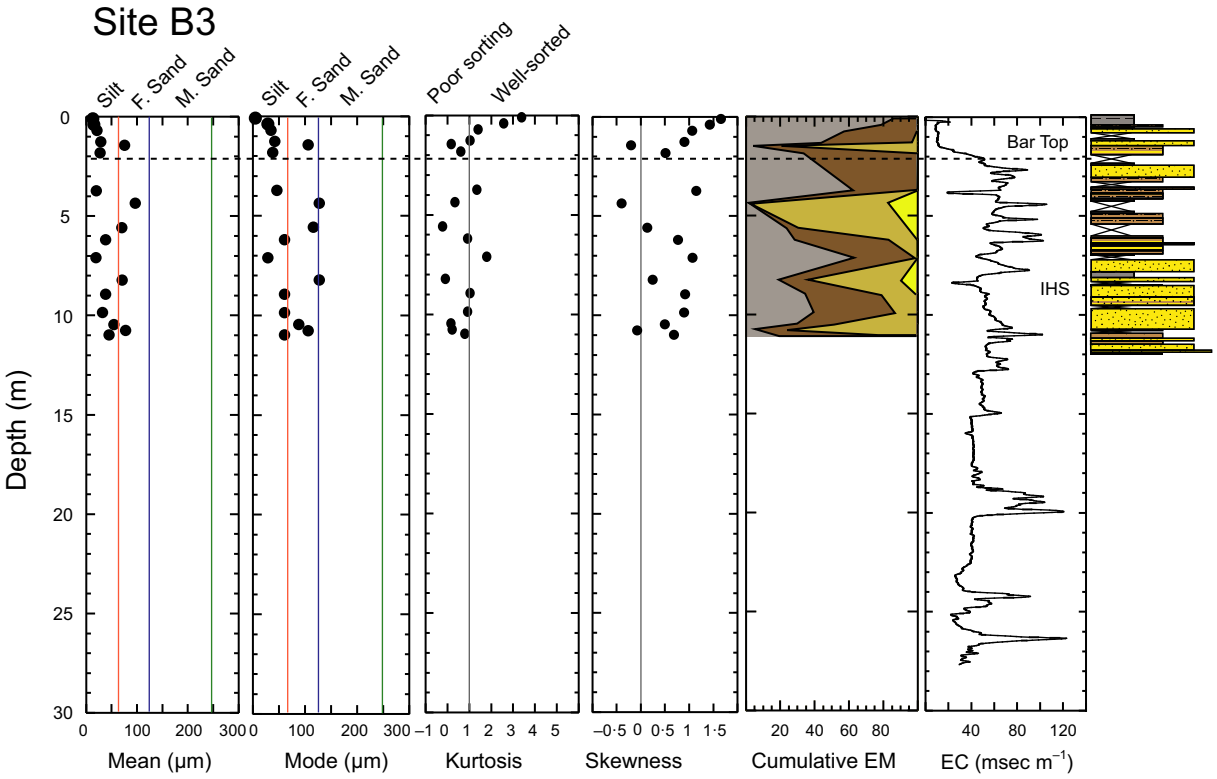

Fig. 7. (Continued).

generally higher, less variable electrical conductivity values in the shallower, finer grained parts of the section. Site W1 does show a trend to fining up-section, but at the same time there are repeated interbeds of silt with poor sorting (low kurtosis), as recognized from the grain-size analysis and frequent peaks in the electrical conductivity log (Fig. 8). It is only below 19 m that generally low conductivity values are established, together with massive sands in the visual core description and a dominance of EM4.

Lithology in the channel plug

Not surprisingly, the channel plug sites (R sites) show a contrast with the point-bar sediments. These sites contain very little sandy sediment at any level (Fig. 9). Sites R1 and R2 show a similar stratigraphy, being very muddy in the top 6 m and 9 m thick, respectively. Below those levels the sediment becomes more silty. This is shown as a step to lower conductivity values in the electrical conductivity logs that correlate well with the grain-size analysis (Fig. 9). It is noteworthy that conductivity values at both sites fall in a smooth fashion below the top few metres, but remain quite high relative to the *ca* 20 milliSiemens/m values associated with the sand-rich beds in the point bar. Based on these data alone there is reason to believe that below 15 m at Site R1 and *ca* 18 m at Site R2 the sediment might be more sandy and relatively homogenous. In contrast, Site R3 has consistent evidence for fine-grained sediment through the section down to 26 m depth (Fig. 9), with only sporadic intervals of fine sand. The mean grain size is silt throughout, with a brief interval of fine sandy (EM3) sediment at 18 to 20 m depth. Kurtosis indicates poor sorting except in the very finest grained sections. The electrical conductivity logs

Fig. 8. Downhole plots of grain-size variability at the bar tail sites W1, W2 and W3. See Figs 1 and 7 for location. The mean, mode, kurtosis and skewness of the sediments from each site for which grain-size characteristics were measured are displayed. A further column shows the breakdown of end members derived by processing through *AnalySize* software, as well as the electrical conductivity downhole log (electrical conductivity). All of these parameters are compared with the visual core description shown on the right-hand side of each figure.

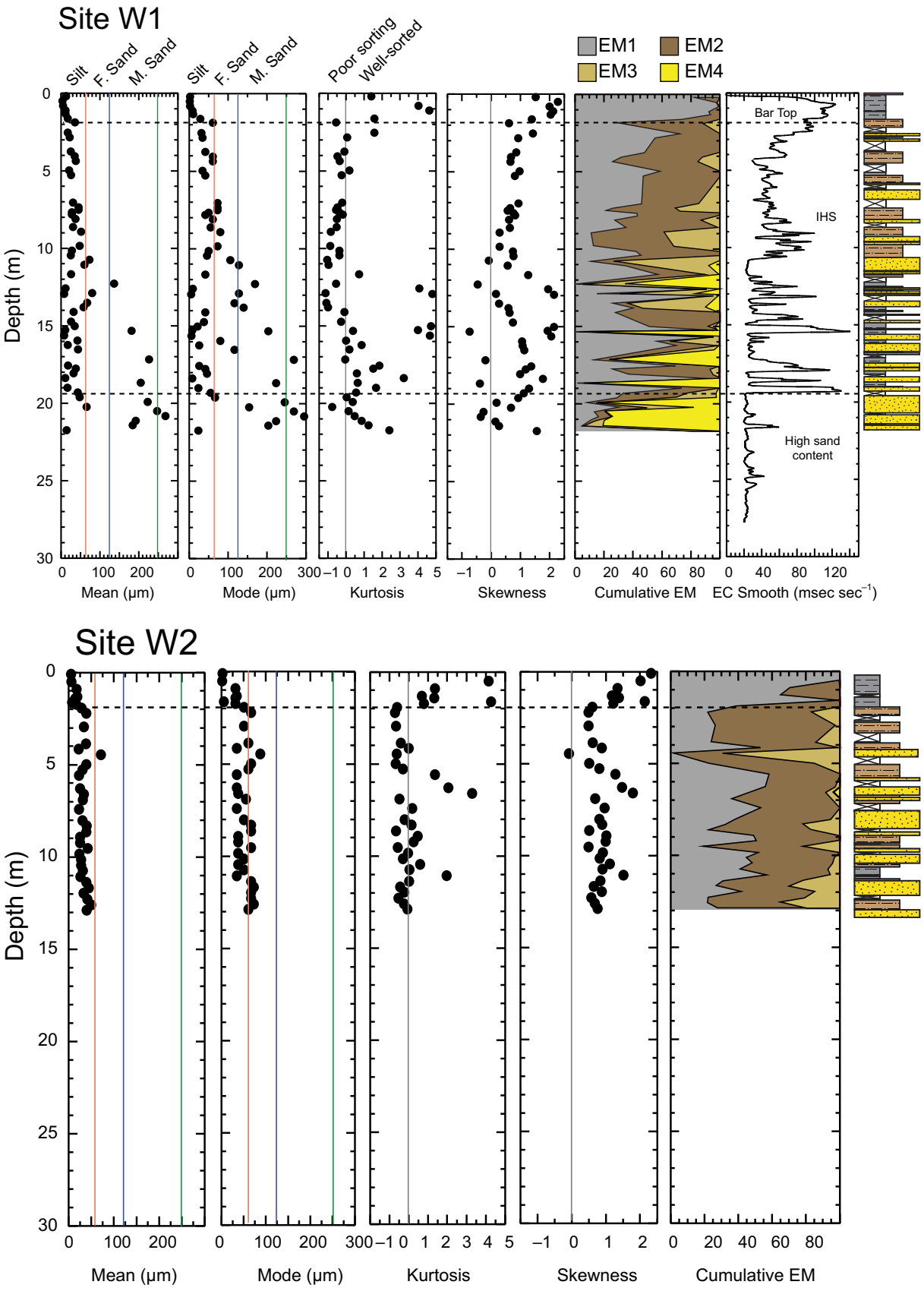

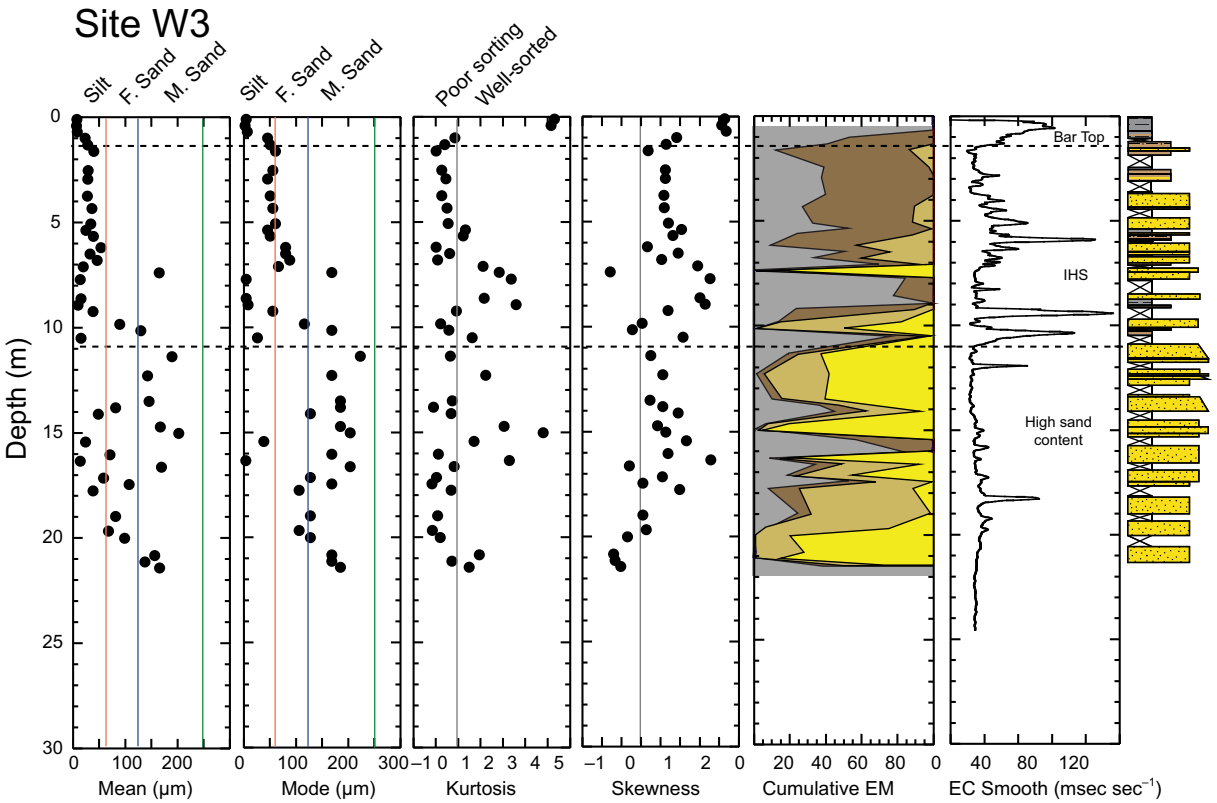

Fig. 8. (Continued).

clearly show two cycles (17 to 24 m and 0 to 13 m; Fig. 9) that imply coarsening-upward above the slightly coarser-grained section below 24 m. These trends do correlate with such trends in the grain-size data but the variations are more subtle (Fig. 9).

Thus, a general pattern can be seen across the point bar in which the silty bar top and silt-fine sand dominated IHS become thicker away from the early apex and towards the final apex area at the expense of a medium sand dominated lower bar unit (Fig. 10). The trend shows a pronounced increase as the bar geometry changes to a compound form. This trend is also seen away from the early apex to the bar tail but more generally affects the youngest accretionary units in the point bar.

DISCUSSION

Light detection and ranging imagery

The digital elevation model (DEM) data clearly show that the False River point bar formed largely by lateral migration perpendicular to the dominant flow in the Mississippi River for much of its growth after experiencing strong rotation of the apex trajectory, from more north to south in the earliest phases to ENE to WSW in the latter stage (Fig. 2). This trend indicates that the point bar was not strongly confined either by the Pleistocene incised valley or by lithology changes in the floodplain.

Controls on grain size

Simple models for grain size and sorting in meander systems typically predict fining upward at any given point, as well fining downstream of the apex. These predictions were tested to see whether they are consistent with the data from False River within the limitation of the sampling here. Because coring was often limited to the upper part of the section, the grain-size analyses do not always reveal the full variability and are biased against the coarser, better sorted sediment at the base of each section that is often shown only by electrical conductivity logging.

Fining up-section is widely recognized, together with increasing variability in the grain-size mode (Fig. 11A). However, the trends tend

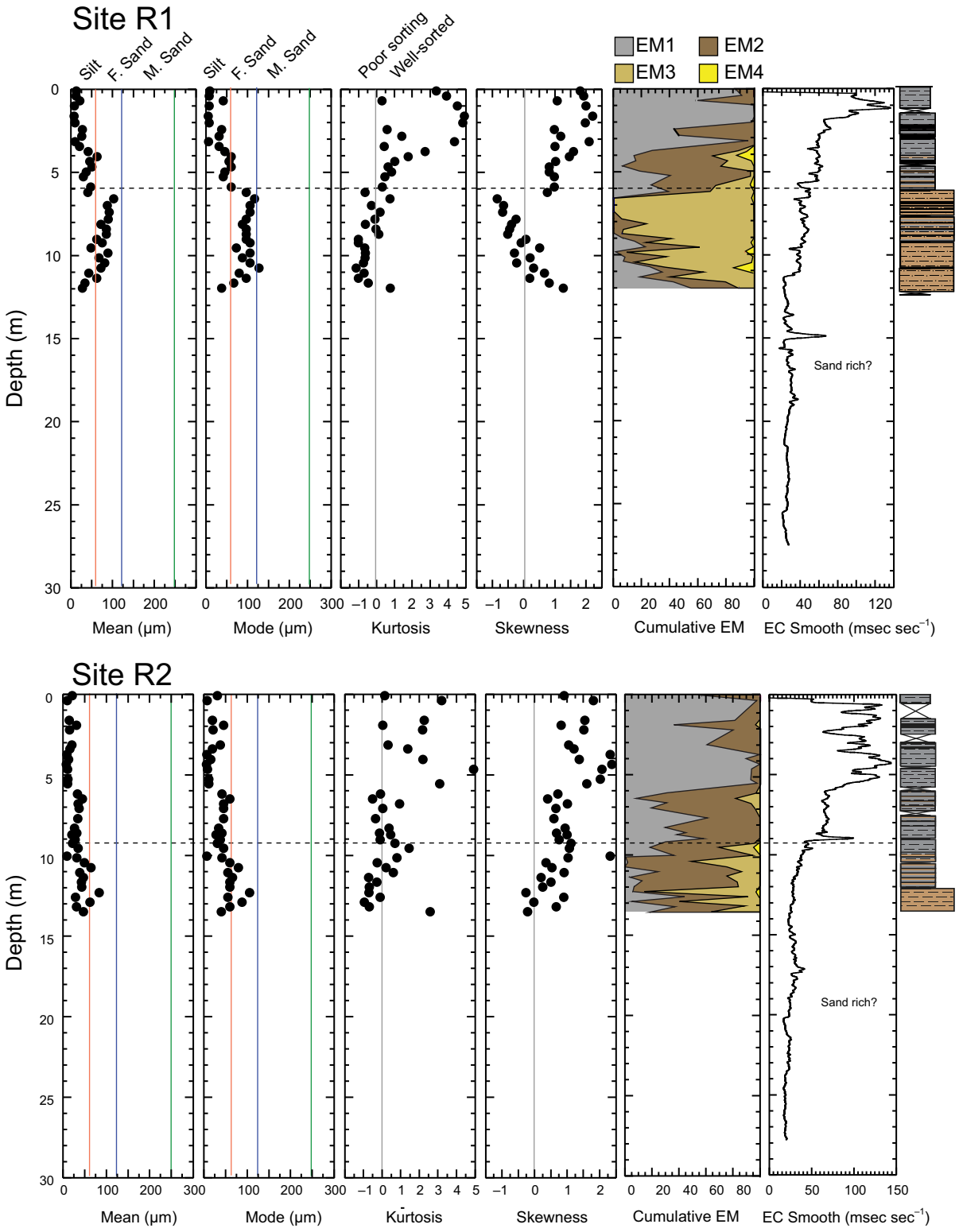

Fig. 9. Downhole plots of grain-size variability at the channel plug sites R1, R2 and R3. See Figs 1 and 2 for location. The mean, mode, kurtosis and skewness of the sediments from each site for which grain-size characteristics were measured are displayed. A further column shows the breakdown of end members derived by processing through *AnalySize* software, as well as the electrical conductivity downhole log (electrical conductivity). All of these parameters are compared with the visual core description shown on the right-hand side of each figure. Numbers 1, 2 and 3 in the electrical conductivity column represent three coarsening-upward cycles.

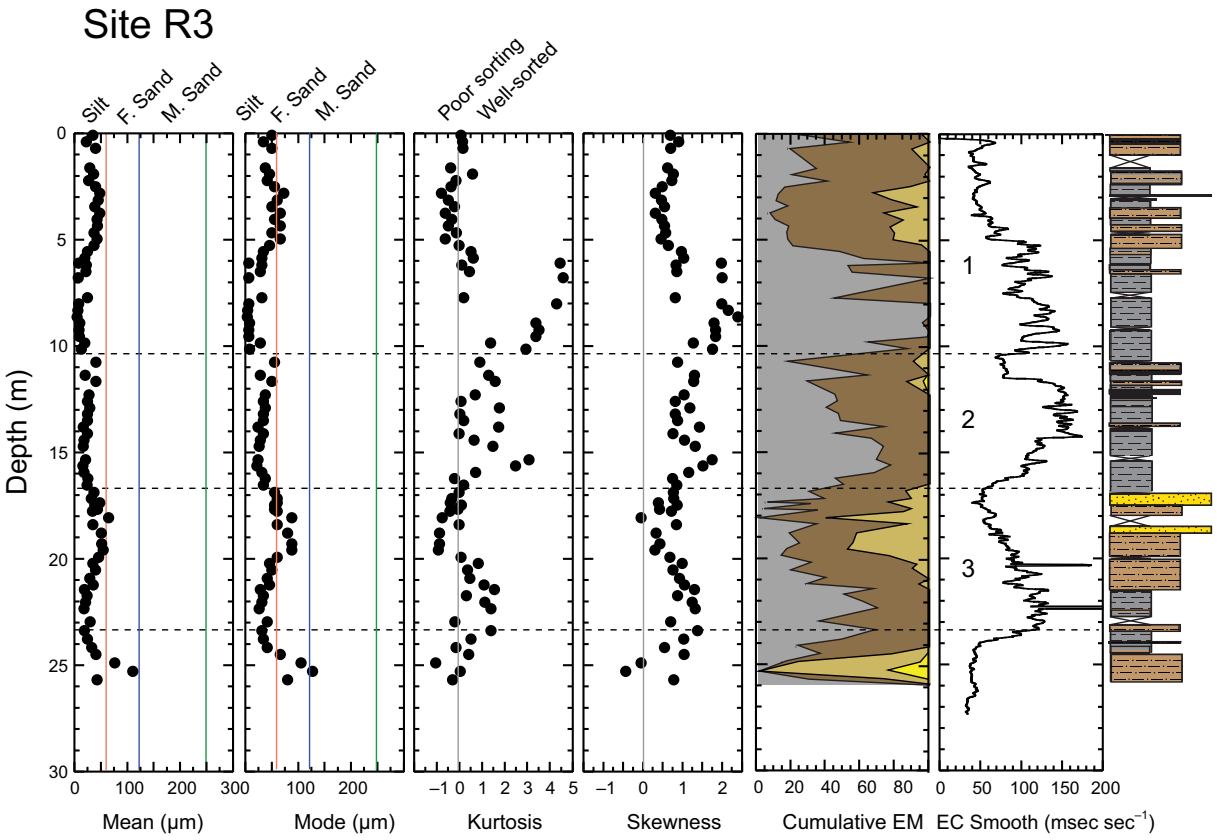

Fig. 9. (Continued).

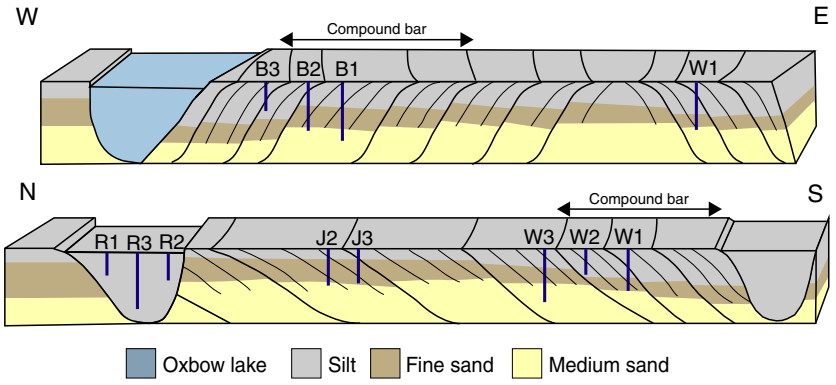

Fig. 10. Block diagrams oriented north–south and east–west across the point bar summarizing variations in sediment type across the False River point bar as constrained by this study.

to be noisier and less well-defined than the fining up seen in the much smaller Esk River point bars of 3 to 4 m thickness total (Bridge *et al.*, 1995), but consistent with the lack of clear fining-upward pattern found in other examples such as the Jurassic Morrison Formation of Utah (Hartley *et al.*, 2015). There is a marked increase in grain size below *ca* 9 to 11 m depth at several sites across the point bar. Nonetheless, fine-grained material is present to the deepest levels sampled, and is not restricted to the upper few metres. Because the early apex (J sites) was not cored as deeply as the other areas this fining-upward trend is only known to extend to *ca* 13·2 m depth, although the electrical conductivity logs are consistent with an increasingly sandy lower section, in accordance with simple bar models. It is noteworthy that at the deepest levels the bar tail (W sites) shows consistently coarser sediments than at the terminal apex (B sites) where the mode rarely is in excess of 150 μm. Electrical conductivity logging at Site

B3, the youngest site, points to greater amounts of fine-grained material down to almost 28 m, contrasting with the older Sites B1 and B2 at the terminal apex. This argues for the finer sediment and lower energy flow conditions being limited largely to the final phase of accretion of this sub-section and prior to reorientation. The data are thus mostly in accordance with the fining-upward model, with the exception of the sediment deposited in the latter stage of construction after the establishment of the compound geometry (Site W1 and the B Sites).

Regarding changes in sorting up-section there are negative kurtosis values throughout the cores but the frequency of the better sorted sediment increases below *ca* 6 m (Fig. 11B). Sediment deeper in the point bar, below the IHS tends to be better sorted, with the highest kurtosis values seen at 13 to 16 m depth in the bar tail (W sites), but not at the terminal apex (B sites). Deeper in the section high kurtosis values continue to be observed but below a maximum at 13 to 16 m. Below 18 m there is a gradual reduction in the number of poorly sorted sediments and especially below 21 m depth kurtosis does not fall below −0·5.

Lateral variability

In order to determine whether sediments really fine around the meander in the way predicted by simple models, the location of each site relative the apex at the time of sedimentation must be accounted for (Fig. 2). This is not a simple matter since part of the earlier point bar is eroded as rotation and re-orientation occurred, thus introducing uncertainty. However, the tight bend seen in the earliest parts of the point bar provides confidence of where the apex was at that point. Enough of the bar is preserved to allow a good estimate to be made of where the apex was at any given time, so that the position of each coring site can be roughly positioned relative to the apex of the time. After establishment of a compound point bar there are two or more active apices at any given time. The distance parallel to the scroll bars from each apex to the drill site was measured, with positive values being given for downstream distance and negative for upstream. The apex locations shown in Fig. 2 are defined at the end of each sub-unit and so the distance from a site within a given unit was measured along the scroll bars and then projected to the final apex location. Site W3 is located furthest downstream from its apex, at *ca* 4 km. Figure 12A shows the grain-size mode for each site with the bar top removed because this fine-grained cover is common to all of the sites and the expected differences would be limited to the IHS and lower bar. It is clear that there is wide scatter of values at each site, although the coarsest modes are seen at Site W1, contrary to the predictions of a simple bar. It should however be noted that the IHS is thicker at Site W1 than at upstream sites (Fig. 8),

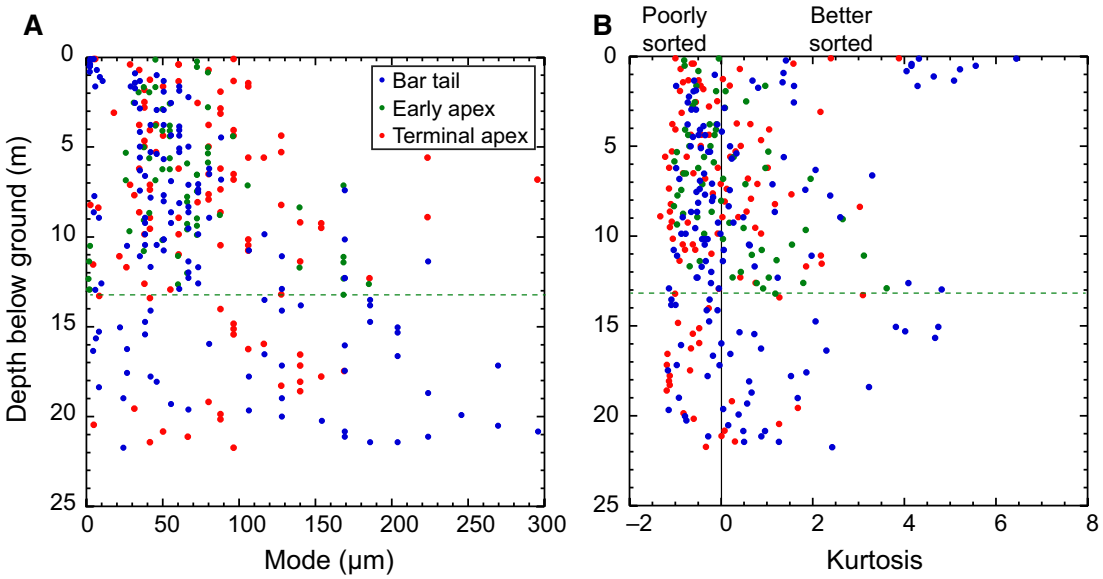

Fig. 11. Plot of: (A) grain-size mode versus depth below the modern ground surface at the three point-bar study areas; and (B) kurtosis versus depth. Coarsening downward is best displayed in the bar tail (W) localities.

which does follow the predictions of simple models but is similar to observations from the smaller Esk River example (Bridge *et al.*, 1995). Deviations from the basic model may be explained by the local irregularities in the compound bar mode of construction. Sites W2, B1 and J3 show generally less scatter and finer grain size (Fig. 12A), but this probably reflects the shallower penetration at each site rather than the absence of coarser sediment deeper in the section. The generally fine-grained character at the terminal apex (B sites) is consistent with their location within the compound bar and close to the end of construction of that sub-unit. Little coherent variability can be detected either in the range of mode sizes, or in the average mode for each site downstream of the apex. This trend contrasts with the well-defined downstream fining seen in the Jurassic Scalby Formation (Ghinassi & Ielpi, 2015), in the modern Peace River of Alberta (Smith *et al.*, 2009). The result at False River is more similar to data from the Ferron Sandstone of Utah which shows some coarsening downstream towards the bar apex and fining downstream of that point, but only in some of the measured meander scrolls (Wang & Bhattacharya, 2017). Instead, the best measured part of that exposure showed little coherent variation, albeit in a channel just 2 to 3 m deep.

Likewise, kurtosis does not show a clear trend downstream (Fig. 12B). The highest valued (best sorted) sediments are again seen at Site W1. This is not entirely a function of coring depth because the highest kurtosis values at that place are not from the base of the section but in the 13 to 16 m depth range. This suggests that downstream fining and sorting is not very strong in the IHS at least.

High energy flow during bar reorientation may also have eroded sandier deposits initially present at Sites W1 and B3. The tendency of these sites to be finer grained and poorly sorted is noteworthy and points to these sediments being deposited under lower energy conditions following reorientation.

The channel plug

The channel plug sites are not correlated to those in the point bar itself because it is clear that this post-dates bar construction and represents the infilling of the old channel. The existence of the modern oxbow lake shows that this process is ongoing and incomplete, although admittedly altered by the presence of an anthropogenic levée system on the modern Mississippi River, and provides the context to understand the sediments recovered. The three coarsening-upward cycles seen at Site R3 are reminiscent of progradational sequences in deltaic settings (Elliott, 1974) and are suggestive of sedimentation from small-scale delta lobes being built

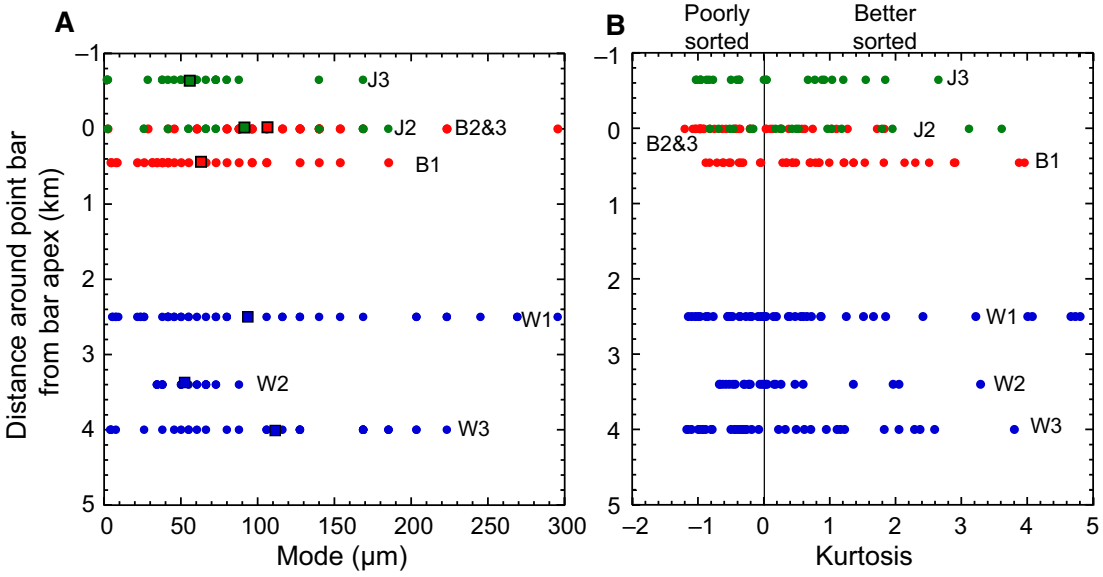

Fig. 12. Plot of: (A) grain-size mode against location on the bar relative the apex at the time of sedimentation. See Fig. 1 for the location of the apex during the accumulation of each stage. Square symbol shows the average value for each site. Data from the bar top are excluded from this plot.

from the connecting remnant channel into the oxbow lake. The oxbow lake is not filled until the top of the third sequence in this place.

Reservoir properties

The grain-size data presented above can be used to assess the quality of these deposits as potential hydrocarbon reservoirs. Ideally a good hydrocarbon reservoir would be relatively coarse-grained and well-sorted, in order to maximize the porosity and permeability characteristics (Ajdukiewicz & Lander, 2010). This study can be used as an analogue for rocks in the ancient that are producing hydrocarbons. As noted above, there is a generally recognized fining up-section in each location, so that the better reservoir rocks would be located at the bottom of the point bar. There is no simple trend to improving reservoir quality around the point bar downstream of the apex at any given time, although reservoir quality deteriorates after the establishment of the compound bar geometry.

Kurtosis and the grain-size mode are critical controls on potential reservoir quality. A significant number of the sediments analyzed are rather fine-grained and well-sorted but would not make good reservoirs nonetheless (Fig. 13). There are a substantial number of sediments analyzed by laser particle size methods, particularly in the channel plug and in terminal apex, which are relatively fine–medium grained but rather poorly sorted. A relatively modest number of the coarser grained sediments show a tendency to better sorting and represent superior reservoir rocks. It is likely that the relatively small number of these sediments reflect the fact that coring did not penetrate to the base of the section. Many of the best quality sands measured are located in the bar tail area (W sites), with relatively few found in the bar apex (B sites). The relative dearth of high quality sands in the early apex (J sites) is mostly a product of the shallow coring in that location because the electrical conductivity logs were supportive of the section fining upward.

The IHS in the early apex region is relatively thin. The initial concept that reservoir quality might decrease in the downstream part of the bar can be tested by looking only at data from the W sites, as shown in Fig. 14. There are a fair number of relatively good quality reservoir sediments particularly at Sites W1 and W3 (Fig. 14). The lack of such material at Site W2 probably reflects the fact that this is only drilled to a depth of *ca* 13 m. Electrical conductivity logging shows that reservoir quality is much better at depth at Site W3 than it is at site W1. The IHS at Site W1 extends down beyond 19 m, whereas at Site W3 the IHS bottoms out at *ca* 11 m. Below that level the section is dominated by relatively high quality sands. In contrast, the

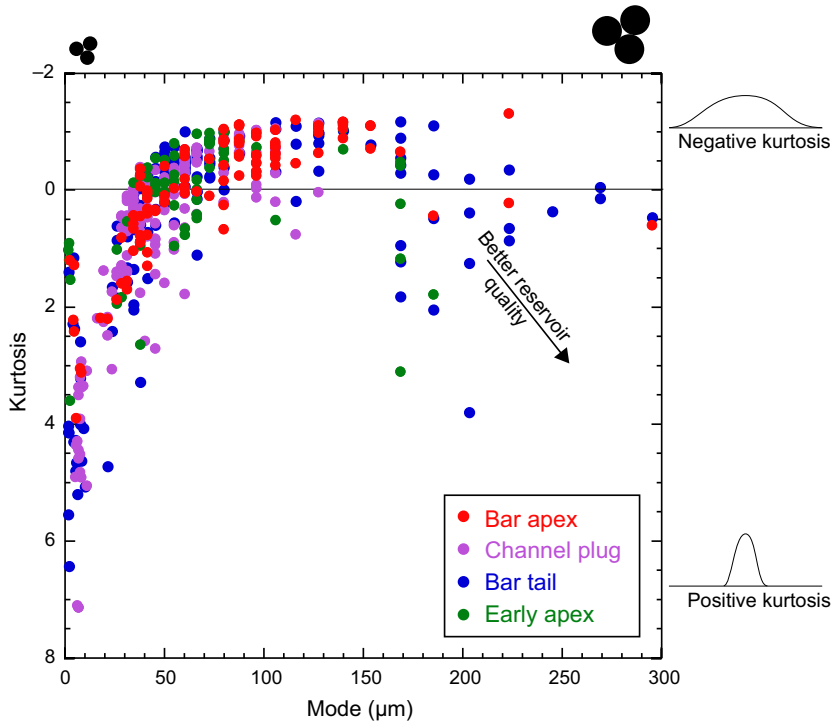

Fig. 13. Plot of kurtosis versus mode for all sites in the point bar and channel plug. Good quality sands are found at all point-bar locations but not in the channel plug.

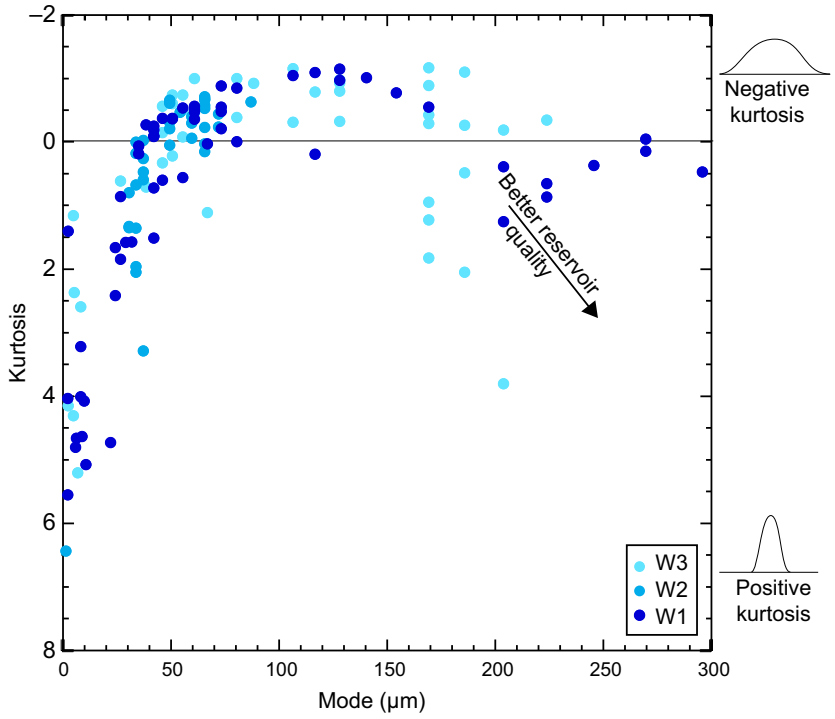

Fig. 14. Plot of kurtosis versus mode for the three sites in the bar tail area. High quality reservoir sands are found at Sites W1 and W3, i.e. at both the older and younger sites in this area. The lack of good sands at Site W2 is most likely to reflect limited depth of coring.

volume of high quality sand at W1 is rather low. This distinction between Sites W3 and W1 probably reflects the establishment of the compound bar geometry and is not simply linked to the distance from the bar apex (Fig. 12). In the compound bar mode local high energy current flow may have eroded back into the south-west portion of the bar and created multiple apices resulting in the poor sorting and fine grain sizes observed at Site W1.

Can data from this study be used in a predictive fashion to predict location within a point bar based on limited sub-surface samples? Small samples, spanning tens of centimetres would not be useful because all lithologies can be found at most locations, but cores of 10 m or more length would provide useful clues as to where in the point bar the drilling was occurring. A very silty or muddy long core with no significant sand would require the samples to be from the channel plug. A silty–muddy core with frequent but thin (10 to 20 cm) interbeds of fine sand would probably be from the edges of the point bar, especially in the bend apex shortly before final cut-off or a downstream location (Fig. 10). Massive, thick-bedded sands (beds >25 cm) would be harder to confidently place but are more likely to be from the apex or upstream parts deposited during early stages of point-bar construction, prior to the switch to a compound morphology. The bar top in all locations is muddy and silty but is only a few metres thick and could be identified in a core long enough to also penetrate the IHS.

The overall depositional model can be conceptualized as a block model (Fig. 15). The progression of meander geometry from a simple loop into a compiund form with several simultaneous active apices is envisaged as being a crucial transition. Current velocity, which controls transport capacity is reduced as the overall meander breaks down a series of small systems, resulting in the deposition of small, finer grained accretionary units. This may be a characteristic of the largest point-bar systems. While meanders in the Jurassic Scalby Formation show a change from downstream migration to more lateral expansion upsection the meanders remain relatively simple in form and do not share the large-scale rotation seen at False River (Ielpi & Ghinassi, 2014). Likewise, the Permian Warchha Sandstone of Pakistan is envisaged as comprising relatively simple meander geometries, with dominant lateral migration and more sand-rich compositions within the point bar itself, albeit not the oxbow meander cut-off (Ghazi & Mountney, 2009). The False River example shows some differences from the Cretaceous McMurray Formation. Lithological models based on gamma ray data point to a strong downstream fining trend and the persistence of a sandy region upstream of the primary apex, even when a compound form had been

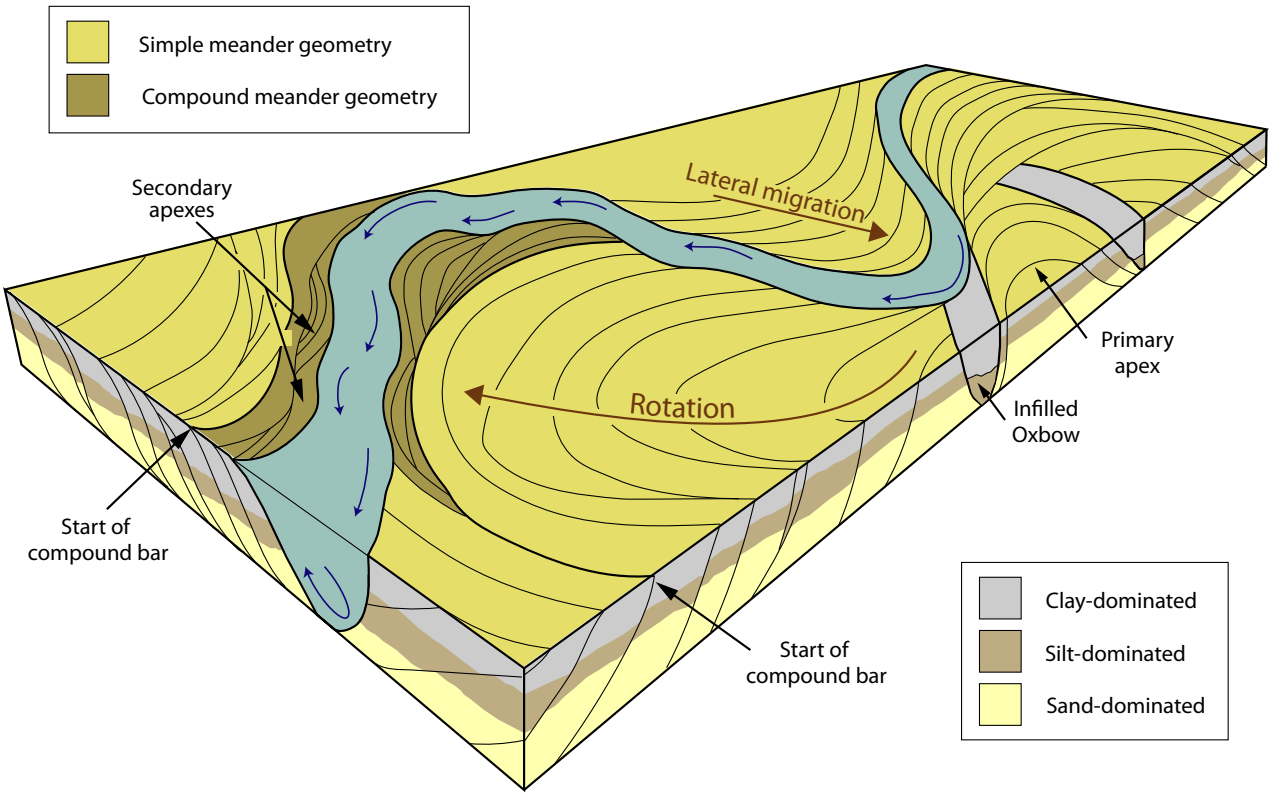

Fig. 15. Summary depositional model of a megascale point-bar complex showing how the change from simple to compound poimt bar causes a shift to generally finer sedimentation in the later stage of point-bar accumulation as the flow around the entire meander is slowed around the multiple secondary apexes. Arrows in stream show zones of maximum current velocity.

achieved (Labrecque *et al.*, 2011). Furthermore, the McMurray Formation does not appear to have the shift to finer grained sediment around the primary apex prior to cut-off. Models based on three-dimensional seismic images of the McMurray Formation do not help to resolve lithological changes in the way that the present data does. However, in general this suggests more simple meander loop morphologies throughout the entire history of accretion but does share the downstream expansion and rotation found in False River (Durkin *et al.*, 2017). Coring data that implies large-shale drapes between accretionary units especially after significant rotation following flood events (Hubbard *et al.*, 2011) are not apparent in the False River example. In general the False River point bar might be expected to have reduced hydrological connectivity between adjacent point-bar complexes compared with existing models from the McMurray Formation because of the greater occurrence of finer facies in compound bar accretionary phase (Hassanpour *et al.*, 2013).

CONCLUSIONS

This study tested simple models of grain-size variability in fluvial point-bar systems at the very largest scale in order to determine whether models developed for small and medium-size systems are applicable at the very largest size. Most of the sediment that was analyzed comes from cores taken in the upper part of the point bar at the bar terminal apex and in the bar tail, as well as an initial apex site, together with the channel plug. Most of the information about the sediment in the deeper part of the section is derived from electrical conductivity logging, which confirms the presence of massive sands in the lower half of the section, especially in the upstream early apex sites (J sites). Most of the sediment analyzed is silty, sandy silt or silty sand, with very little clay found outside the channel plug. End member modelling was able to determine that the range of grain-size variability can be explained by four different grain-size end members.

It is clear that there is a common coarsening down-section at most of the sites. However, sorting does not show such a clear down-section trend, except in the top 9 to 11 m, representing the Inclined Heterolithic Strata (IHS). The IHS is thicker, *ca* 19 m, at Site W1, located in the bar tail and after establishment of a compound bar geometry at the B sites (Fig. 10). There is no clear fining of the sediment downstream of the apex at any given time. Establishment of a compound bar morphology appears to be more critical to controlling sorting and grain size than location on the point bar prior to that time.

The best quality potential reservoir sediments, i.e. the coarsest grain sizes with the best sorting that would be anticipated to have the best fluid flow characteristics are located in the centre of the point bar and accumulated during the time of uni-apex accretion. Quality progressively deteriorates towards the edges, especially at the final apex and in the extreme downstream parts of the bar. This tendency for reservoir quality to reduce downstream is a characteristic shared with smaller, simple point-bar complexes. Furthermore, because the IHS gets thicker downstream the volume of the high quality reservoir sands at the point-bar base will also reduce in that direction. The filled channel plug is particularly noteworthy in being very poor potential reservoir quality.

ACKNOWLEDGEMENTS

We wish to thank ExxonMobil Upstream Research Company for financial support of this project, and especially to Paul Dunn for his intellectual feedback. Betty Woody, Walter Bueche, Gail Roberts, Gary Jewell, Glen Ray Cline, Dutcher Jumonville and J.E. Jumonville are thanked for permitting us to access their land for scientific research. Scott Bergeron and his colleagues at Professional Technical Support Services Inc. did an excellent job in performing much of the rig operation work. Editor Nigel Mountney, Amanda Owen and two anonymous reviewers provided helpful comments that greatly improved the initial submission. We thank Dr. Stephanie K. Davidson for her advice early in the project. Dr. Samuel Bentley from LSU was generous in allowing us access to his grain-size laboratory. We also thank Erinn Buhyoff, Connor Matherne, Claire Jones, Chris Howie and Daniel Babin for their help in the laboratory.

REFERENCES

Ajdukiewicz, J.M. and **Lander, R.H.** (2010) Sandstone reservoir quality prediction: the state of the art. *AAPG Bull.*, **94**, 1083–1091.

Allen, J.R.L. (1963) The Classification of Cross-Stratified Units with Notes on their Origin. *Sedimentology*, **2**, 93–114.

Allen, J.R.L. (1965) A review of the origin and characteristics of recent alluvial sediments. *Sedimentology*, **5**, 89–191.

Alqahtani, F.A., **Johnson, H.D.**, **Jackson, C.A.-L.** and **Som, M.R.B.** (2015) Nature, origin and evolution of a late pleistocene incised valley-fill, sunda shelf, southeast Asia. *Sedimentology*, **62**, 1198–1232.

Blatt, H., **Middleton, G.** and **Murray, R.** (1980) *Origin of Sedimentary Rocks*. Prentice-Hall, Englewood Cliffs, NJ, 782 pp.

Bluck, B.J. (1971) Sedimentation in the meandering River Endrick. *Scott. J. Geol.*, **7**, 93–138.

Blum, M.D. and **Roberts, H.H.** (2012) The mississippi delta region: past, present, and future. *Annu. Rev. Earth Planet. Sci.*, **40**, 655–683.

Blum, M.D. and **Törnqvist, T.E.** (2000) Fluvial responses to climate and sea-level change: a review and look forward. *Sedimentology*, **47**, 2–48.

Bogaart, P.W. and **Van Balen, R.T.** (2000) Numerical modeling of the response of alluvial rivers to Quaternary climate change. *Global Planet. Change*, **27**, 147–163.

Brice, J.C. (1974) Evolution of meander loops. *Bull. Geol. Soc. Am.*, **85**, 581–586.

Bridge, J.S., **Alexander, J.**, **Collier, R.E.L.**, **Gawthorpe, R.** and **Jarvis, J.** (1995) Ground penetrating radar and coring used to document large-scale structures of point-bar deposits in 3D. *Sedimentology*, **42**, 839–852.

Carter, D.C. (2003) 3-D seismic geomorphology: insights into fluvial reservoir deposition and performance, Widuri field, Java Sea. *AAPG Bull.*, **87**, 909–934.

Chatanantavet, P., **Lamb, M.P.** and **Nittrouer, J.A.** (2012) Backwater controls of avulsion location on deltas. *Geophys. Res. Lett.*, **39**, L01402. https://doi.org/10.1029/2011GL05019

Choi, K.S. (2011) External controls on the architecture of inclined heterolithic stratification (IHS) of macrotidal Sukmo Channel: wave versus rainfall. *Mar. Geol.*, **285**, 17–28.

Collinson, J.D. (1986) Alluvial Sediments. In: *Sedimentary Environments and Facies* (Ed. H.G. Reading), pp. 37–81. Blackwell Scientific Publications, Oxford.

Colombera, L., **Yan, N.**, **McCormick-Cox, T.** and **Mountney, N.P.** (2018) Seismic-driven geocellular modeling of fluvial meander-belt reservoirs using a rule-based method. *Mar. Pet. Geol.*, **93**, 553–569.

Constantine, J.A., **McLean, S.R.** and **Dunne, T.** (2010) A mechanism of chute cutoff along large meandering rivers with uniform fl oodplain topography. *Geol. Soc. Am. Bull.*, **122**, 855–869.

Cuevas Martinez, J.L., **Cabrera, L.**, **Marcuello, A.**, **Arbues, P.**, **Marzo, M.** and **Bellmunt, F.** (2010) Exhumed channel sandstone networks within fluvial fan deposits from the Oligo-Miocene Caspe Formation, South-east Ebro Basin (North-east Spain). *Sedimentology*, **57**, 162–189.

Daniel, J.F. (1971) Channel movement of meandering Indiana streams. U.S. Geological Survey.

Diaz-Molina, M. (1993) Geometry and lateral accretion patterns in meander loops: examples from the upper Oligocene-lower

Miocene, Loranca Basin, Spain. In: *Alluvial sedimentation* (Eds M. Marzo and C. Puigdefabregas), *Special publication*, **17**, pp. 115–131. International Association of Sedimentologists/Blackwell, Oxford.

Díez-Canseco, D., **Arz, J.A.**, **Benito, M.I.**, **Díaz-Molina, M.** and **Arenillas, I.** (2014) Tidal influence in redbeds: a palaeoenvironmental and biochronostratigraphic reconstruction of the Lower Tremp Formation (South-Central Pyrenees, Spain) around the Cretaceous/Paleogene boundary. *Sed. Geol.*, **312**, 31–49.

Dreyer, T., **Fält, L.-M.**, **Høy, T.**, **Knarud, R.**, **Steel, R.** and **Cuevas, J.-L.** (1992) Sedimentary Architecture of Field Analogues for Reservoir Information (SAFARI): A Case Study of the Fluvial Escanilla Formation, Spanish Pyrenees. In: *The Geological Modelling of Hydrocarbon Reservoirs and Outcrop Analogue* (Eds S.S. Flint and I.D. Bryant). Blackwell Publishing Ltd, Oxford, UK.

Durkin, P.R., **Boyd, R.L.**, **Hubbard, S.M.**, **Shultz, A.W.** and **Blum, M.D.** (2017) Three-dimensional reconstruction of meander-belt evolution, cretaceous McMurray formation, Alberta foreland basin, Canada. *J. Sed. Res.*, **87**, 1075–1099.

Elliott, T. (1974) Interdistributary bay sequences and their genesis. *Sedimentology*, **21**, 611–622.

Farrell, K.M. (1987) Sedimentology and facies architecture of overbank deposits of the Mississippi River, False River region, Louisiana. In: *Recent Developments in Fluvial Sedimentology, Special publication* (Eds. F.G., Etheridge, R.M., Flores and M.D., Harvey), **39**, pp. 111–120. SEPM, Tulsa.

Fielding, C.R. and **Crane, R.C.** (1987) An application of statistical modelling to the predicton of hydrocarbon recovery factors in fluvial reservoir sequences. In: *Recent Developments in Fluvial Sedimentology* (Eds F.G. Ethridge, R.M. Flores and M.D. Harvey), *SEPM Spec. Publ.*, **39**.

Fisk, H.N. (1947) Fine-grained alluvial deposits and their effects on Mississippi River activity, Mississippi River Commission, Vicksburg, Mississippi.

Foix, N., **Allard, J.O.**, **Paredes, J.M.** and **Giacosa, R.E.** (2012) Fluvial styles, paleohydrology and modern analogues of an exhumed, Cretaceoues fluvial system: Cerro Bacino Formation, Canadon Asfalto Basin, Argentina. *Cretac. Res.*, **34**, 298–307.

Folk, R.L. (1954) The distinction between grain size and mineral composition in sedimentary rock nomenclature. *J. Geol.*, **62**, 344–359.

Folk, R.L. and **Ward, W.C.** (1974) Brazos River bar: a study in the significance of grain size parameters. *J. Sediment. Res.*, **27**, 3–26.

Frascati, A. and **Lanzoni, S.** (2009) Morphodynamic regime and long-term evolution of meandering rivers. *J. Geophys. Res.*, **114**, F02002. https://doi.org/10.1029/2008JF001101

Fustic, M. (2007) Stratigraphic dip analysis- a novel application for detailed geological modeling of point bars and predicting bitumen grade, McMurray Formation, Muskeg River Mine, Northeast Alberta. *Nat. Resour. Res.*, **16**, 31–43.

Fustic, M., **Hubbard, S.M.**, **Spencer, R.**, **Smith, D.G.**, **Leckie, D.A.**, **Bennett, B.** and **Larter, S.** (2012) Recognition of down-valley translation in tidally influenced meandering fluvial deposits, Athabasca Oil Sands (Cretaceous), Alberta, Canada. *Mar. Pet. Geol.*, **29**, 219–232.

Gesch, D., **Oimoen, M.**, **Greenlee, S.**, **Nelson, C.**, **Steuck, M.** and **Tyler, D.** (2002) The National Elevation Dataset. *J. Am. Soc. Photogrammetr. Remote Sens.*, **68**, 1.

Ghazi, S. and **Mountney, N.P.** (2009) Facies and architectural element analysis of a meandering fluvial succession: the Permian Warchha Sandstone, Salt Range, Pakistan. *Sed. Geol.*, **221**, 99–126.

Ghinassi, M. and **Ielpi, A.** (2015) Stratal architecture and morphodynamics of downstream-migrating fluvial point bars (Jurassic Scalby Formation, U.K.). *J. Sediment. Res.*, **85**, 1123–1137.

Ghinassi, M., **Ielpi, A.**, **Aldinucci, M.** and **Fustic, M.** (2016) Downstream-migrating fluvial point bars in the rock record. *Sed. Geol.*, **334**, 66–96.

Gibling, M.R. (2006) Width and thickness of fluvial channel bodies and valley fills in the geological record: a literature compilation and classification. *J. Sediment. Res.*, **76**, 731–770.

Gibling, M.R. and **Rust, B.R.** (1993) Alluvial ridge-and-swale topography: a case study from the Morien Group of Atlantic Canada. In: *Alluvial Sedimentation* (Eds M. Marzo and C. Puigdefabregas), *Spec. Publ.*, **17**, pp. 133–150. International Association of Sedimentologists.

Gibling, M.R., **Tandon, S.K.**, **Sinha, R.** and **Jain, M.** (2005) Discontinuity-bounded alluvial sequences of the southern Gangetic Plains, India: aggradation and degradation in response to monsoonal strength. *J. Sediment. Res.*, **75**, 369–385.

Gouw, M.J.P. (2007) Alluvial architecture of fluvio-deltaic succession: a review with special reference to Holocene setting. *Neth. J. Geosci.*, **86**, 221–227.

Gouw, M.J.P. and **Autin, W.J.** (2008) Alluvial architecture of the Holocene Lower Mississippi Valley (U.S.A.) and a comparison with the Rhine-Muse delta (Netherlands). *Sed. Geol.*, **204**, 106–121.

Hampson, G.J., **Royhan Gani, M.**, **Sahoo, H.**, **Rittersbacher, A.**, **Irfan, N.**, **Ranson, A.**, **Jewell, T.O.**, **Gani, N.D.**, **Howell, J.A.** and **Buckley, S.J.** (2012) Controls on large-scale patterns of fluvial sandbody distribution in alluvial to coastal plain strata: upper Cretaceous Blackhawk Formation, Wasatch Plateau, Central Utah, USA. *Sedimentology*, **59**, 2226–2258.

Hartley, A.J., **Owen, A.**, **Swan, A.**, **Weissmann, G.S.**, **Holzweber, B.I.**, **Howell, J.**, **Nichols, G.** and **Scuderi, L.** (2015) Recognition and importance of amalgamated sandy meander belts in the continental rock record. *Geology*, **43**, 679–682.

Hassanpour, M.M., **Pyrcz, M.J.** and **Deutsch, C.V.** (2013) Improved geostatistical models of inclined heterolithic strata for McMurray Formation, Alberta, Canada. *AAPG Bull.*, **97**, 1209–1224.

Hickin, E.J. (1974) The development of meanders in natural river-channels. *Am. J. Sci.*, **274**, 414–442.

Hooke, J.M. (2008) Temporal variations in fluvial processes on an active meandering river over a 20-year period. *Geomorphology*, **100**, 3–13.

Hubbard, S.M., **Smith, D.G.**, **Nielsen, H.**, **Leckie, D.A.**, **Fustic, M.**, **Spencer, R.J.** and **Bloom, L.** (2011) Seismic geomorphology and sedimentology of a tidally influenced river deposit, Lower Cretaceous Athabasca oil sands, Alberta, Canada. *Am. Asso. Petrol. Geol. Bull.*, **95**, 1123–1145.

Hudson, P.F. and **Kesel, R.H.** (2000) Channel migration and meander-bend curvature in the lower Mississippi River prior to major human modification. *Geology*, **28**, 531–534.

Hülse, P. and **Bentley, S.J.** (2012) A 210Pb sediment budget and granulometric record of sediment fluxes in a subarctic

deltaic system: the Great Whale River, Canada. *Estuar. Coast. Shelf Sci.*, **109**, 41–52.

Ielpi, A. and **Ghinassi, M.** (2014) Planform architecture, stratigraphic signature and morphodynamics of an exhumed Jurassic meander plain (Scalby Formation, Yorkshire, UK). *Sedimentology*, **61**, 1923–1960.

Jackson, R.G. (1976) Depositional model of point bars in the lower Wabash River. *J. Sediment. Petrol.*, **46**, 579–594.

Johnson, S.M. and **Dashtgard, S.E.** (2014) Inclined heterolithic stratification in a mixed tidal fluvial channel: differentiating tidal versus fluvial controls on sedimentation. *Sed. Geol.*, **301**, 41–53.

Julien, P.Y. and **Wargadalam, J.** (1995) Alluvial channel geometry: theory and applications. *J. Hydraul. Eng.*, **121**, 312–325.

Knighton, D. (2014) *Fluvial Forms and Processes: A New Perspective*. Routledge, London.

Labrecque, P.A., **Jensen, J.L.** and **Hubbard, S.M.** (2011) Cyclicity in Lower Cretaceous point bar deposits with implications for reservoir characterization, Athabasca Oil Sands, Alberta, Canada. *Sed. Geol.*, **242**, 18–33.

Lamb, M.P., **Nittrouer, J.A.**, **Mohrig, D.** and **Shaw, J.** (2012) Backwater and river plume controls on scour upstream of river mouths: implications for fluvio-deltaic morphodynamics. *J. Geophys. Res.*, **117**, F01002. https://doi.org/10.1029/2011JF002079

Leopold, L.B., **Wolman, M.G.** and **Miller, J.P.** (1964) *Fluvial Processes in Geomorphology*. W.H. Freeman, San Francisco, CA, 522 pp.

Marriott, S.B. and **Wright, V.P.** (1993) Palaeosols as indicators of geomorphic stability in two Old Red Sandstone alluvial suites, South Wales. *J. Geol. Soc.*, **150**, 1109–1120.

McCall, W. (1996) Electrical conductivity logging to determine control of hydrocarbon flow paths in alluvial sediments. In: Outdoor Action Conference. NGA 1996. National Groundwater Association Annual Meeting, Las Vegas, NV.

McCarthy, P.J., **Martini, I.P.** and **Leckie, D.A.** (1997) Anatomy and evolution of a Lower Cretaceous alluvial plain: sedimentology and palaeosols in the upper Blairmore Group, south-western Alberta, Canada. *Sedimentology*, **44**, 197–220.

McGowen, J.H. and **Garner, L.E.** (1970) Physiographic features and stratification types of coarse-grained point bars; Modern and ancient examples. *Sedimentology*, **14**, 77–111.

Miall, A.D. (1985) Architectural-element analysis: a new method of facies analysis applied to fluvial deposits. *Earth Sci. Rev.*, **22**, 261–308.

Miall, A.D. (2006) Reconstructing the architecture and sequence stratigraphy of the preserved fluvial record as a tool for reservoir development: a reality check. *AAPG Bull.*, **90**, 989–1002.

Musial, G., **Reynaud, J.Y.**, **Gingras, M.K.**, **Fenies, H.**, **Labourdette, R.** and **Parize, O.** (2012) Subsurface and outcrop characterization of large tidally influenced point bars of the Cretaceous McMurray Formation (Alberta, Canada). *Sed. Geol.*, **279**, 156–172.

Nanson, G.C. (1980) Point bar and floodplain formation of the meandering Beatton River, Northeastern British Columbia, Canada. *Sedimentology*, **27**, 3–29.

Parker, G. and **Andrews, E.D.** (1986) On the time development of meander bends. *J. Fluid Mech.*, **162**, 139–156.

Parker, G., **Sawai, K.** and **Ikeda, S.** (1982) Bend theory of river meanders. Part 2. Nonlinear deformation of finite-amplitude bends. *J. Fluid Mech.*, **115**, 303–314.

Parker, G., **Shimizu, Y.**, **Wilkerson, G.V.**, **Eke, E.C.**, **Abad, J.D.**, **Lauer, J.W.**, **Paola, C.**, **Dietrich, W.E.** and **Voller, V.R.** (2010) A new framework for modeling the migration of meandering rivers. *Earth Surf. Proc. Land.*, **36**, 70–86.

Paterson, G.A. and **Heslop, D.** (2015) AnalySize: new methods for unmixing sediment grain-size data. *Geochem. Geophys. Geosyst.*, **16**, 4494–4506.

Prins, M.A. and **Weltje, G.J.** (1999) End-member modeling of siliciclastic grain-size distributions: the late Quaternary record of aeolian and fluvial sediment supply to the Arabian Sea and its paleoclimatic significance. In: *Numerical Experiments in Stratigraphy: Recent Advances in Stratigraphic and Sedimentologic Computer Simulations* (Ed. J. Harbaugh), *Special Publication*, **62**, pp. 91–111. Society for Sedimentary Geology, Tulsa, OK.

Revil, A. and **Glover, P.W.J.** (1998) Nature of surface and electrical conductivity in natural sands, sandstones, and clays. *Geophys. Res. Lett.*, **25**, 691–694.

Robinson, B.A. (2013) Recent (circa 1998 to 2011) channel-migration rates of selected streams in Indiana, U.S. Geological Survey.

Saucier, R.T. (1969) Geological Investigation of the Mississippi River area, Artonish to Donaldsonville, LA, U.S. Army Corps of Engineers, Waterways Experiment Station, Vicksburg, Mississippi.

Saucier, R.T. (1974) Quaternary geology of the Lower Mississippi Valley. *Arkan. Archeol. Surv. Res. Ser.*, **6**.

Schumm, S. (1993) River response to baselevel change: implications for sequence stratigraphy. *J. Geol.*, **101**, 279–294.

Schwenk, J., **Lanzoni, S.** and **Foufoula-Georgiou, E.** (2015) The life of a meander bend: connecting shape and dynamics via analysis of a numerical model. *J. Geophys. Res.*, **120**, 690–710.

Shanley, K.W. (2004) Fluvial reservoir description for a giant, low-permeability gas field: Jonah field, Green River Basin, Wyoming, U.S.A. In: *Jonah Field: Case Study of a Giant Tight-gas Fluvial Reservoir* (Eds J.W. Robinson and K.W. Shanley), *AAPG Studies in Geology*, **52**, 159–182.

Shiers, M., **Mountney, N.**, **Hodgson, D.** and **Cobain, S.** (2014) Depositional Controls on Tidally Influenced Fluvial Successions, Neslen Formation, Utah, USA. *Sed. Geol.*, **311**, 1–16.

Smith, D.G. (1985). Modern Analogues of the McMurray Formation Channel Deposits, Sedimentology of Meso-tidal-influenced Meandering River Point Bars with Inclined Beds of Alternating Mud and Sand, Alberta Oil Sands Technology and Research Authority, Calgary.

Smith, D.G. (1987) Meandering river point bar lithofacies models: modern and ancient examples compared. In: *Recent Developments in Fluvial Sedimentology* (Eds F.G. Ethridge, R.M. Flores and M.D. Harvey), *Special Paper*, **39**, pp. 83–93. The Society of Economic Paleontologists and Mineralogists (SEPM).

Smith, R.M. (1990) Alluvial paleosols and pedofacies sequences in the Permian Lower Beaufort of the southwestern Karoo Basin, South Africa. *J. Sediment. Res.*, **60**, 258–276.

Smith, D.G., **Hubbard, S.M.**, **Leckie, D.** and **Fustic, M.** (2009) Counter point bar deposits: lithofacies and reservoir significance in the meandering modern Peace

River and ancient McMurray Formation, Alberta, Canada. *Sedimentology*, **56**, 1655–1669.

Smith, D.G., **Hubbard, S.M.**, **Lavigne, J.R.**, **Leckie, D.A.** and **Fustic, M.** (2011) Stratigraphy of counter-point-bar and eddy-accretion deposits in low-energy meander belts of the Peace–Athabasca Delta, northeast Alberta, Canada. In: *From River to Rock Record: The Preservation of Fluvial Sediments and Their Subsequent Interpretation* (Eds S. Davidson, S. Leleu and C.P. North), *SEPM Spec. Publ.*, **97**, 143–152.

Sternberg, H.O.R. (1956) *A Contribution to the Geomorphology of the False River Area*. PhD, Louisiana State University, Baton Rouge, LA, 169 pp.

Tanner, W.F. (1991) Suite statistics: The hydrodynamic evolution of the sediment pool. In: *Principles, Methods, and Application of Particle Size Analysis* (Ed. J.P.M. Syvitski), pp. 225–236. Cambridge University Press, Cambridge, UK.

Thomas, R.G., **Smith, D.G.**, **Wood, J.M.**, **Visser, J.**, **Calverley-Range, E.A.** and **Koster, E.H.** (1987) Inclined heterolithic stratification-terminology, description, interpretation and significance. *Sed. Geol.*, **53**, 123–179.

Toonen, W.H., **Kleinhans, M.G.** and **Cohen, K.M.** (2012) Sedimentary architecture of abandoned channel fills. *Earth Surf. Proc. Land.*, **37**, 459–472.

Tornqvist, T.E. (1993) Holocene alternation of meandering and anastomosing fluvial systems in the Rhine-Meuse Delta (Central Netherlands) controlled by sea-level rise and subsoil erodibility. *J. Sediment. Res.*, **63**, 683–693.

Wang, J. and **Bhattacharya, J.P.** (2017) Plan-view Paleochannel Reconstruction of Amalgamated Meander Belts, Cretaceous Ferron Sandstone, Notom Delta, South-central Utah, USA. *J. Sediment. Res.*, **88**, 58–74.

Weltje, G.J. and **Prins, M.A.** (2003) Muddled or mixing? Inferring palaeoclimate from size distributions of deep sea clastics. *Sed. Geol.*, **162**, 39–62.

Weltje, G. and **Prins, M.** (2007) Genetically meaningful decomposition of grain-size distributions. *Sed. Geol.*, **202**, 409–424.

Werren, E.G., **Shew, R.D.**, **Adams, E.R.** and **Stancliffe, R.J.** (1990) Meander-belt reservoir geology, mid-dip Tuscaloosa, Little Creek field, Mississippi. In: *Sandstone Petroleum Reservoirs* (Eds J.H. Barwis, J.G. McPherson and R.J. Studlick), pp. 85–107. Springer, Berlin.

Wightman, D.M. and **Pemberton, S.G.** (1997) The lower Cretaceous (Aptian) McMurray Formation: an overview of the McMurray area, northeastern Albert. In: *Petroleum Geology of the Cretaceous Lower Manville Group: Western Canada* (Eds G.S. Pemberton and D.P. James), *Memoir*, **18**, pp. 312–344. Canadian Society of Petroleum Geologists.

Willis, B.J. and **Tang, H.** (2010) Three-dimensional connectivity of point-bar deposits. *J. Sediment. Res.*, **80**, 440–454.

Wood, J.M. (1989) Alluvial architecture of the upper Cretaceous Judith River formation, Dinosaur Provincial Park, Alberta, Canada. *Bull. Can. Pet. Geol.*, **37**, 169–181.

Yan, N., **Mountney, N.P.**, **Colombera, L.** and **Dorrell, R.M.** (2017) A 3D forward stratigraphic model of fluvial meander-bend evolution for prediction of point-bar lithofacies architecture. *Comput. Geosci.*, **105**, 65–80.

Zinger, J.A., **Rhoads, B.L.** and **Best, J.L.** (2011) Extreme sediment pulses generated by bend cutoffs along a large meandering river. *Nat. Geosci.*, **4**, 675–678.

Manuscript received 19 March 2018; revision accepted 31 July 2018